Magnetic separation of ilmenite used as an oxygen carrier in fluidized bed combustion

Bachelor's thesis in Chemical Engineering

Ignacio Lamarca

BACHELOR'S THESIS 2021

Magnetic separation of ilmenite used as an oxygen carrier in fluidized bed combustion

Ignacio Lamarca

Department of Chemistry and Chemical Engineering

Division of Energy and Materials

CHALMERS UNIVERSITY OF TECHNOLOGY

Gothenburg, Sweden 2021

Magnetic separation of ilmenite used as an oxygen carrier in fluidized bed combustion

IGNACIO LAMARCA BARBA

Supervisor: Pavleta Knutsson, Department of Chemistry and Chemical Engineering
Examiner: Britt-Marie Steenari, Department of Chemistry and Chemical Engineering

Bachelor's thesis 2021
Department of Chemistry and Chemical Engineering
Division of Energy and Materials
Chalmers University of Technology
SE-412 96 Gothenburg
Telephone + 46 (0)31-772 1000

Gothenburg, Sweden 2021

Magnetic separation of ilmenite used as an oxygen carrier in fluidized bed combustion
IGNACIO LAMARCA BARBA
Department of Chemistry and Chemical Engineering
Division of Energy and Materials
Chalmers University of Technology

Abstract

This bachelor thesis studies how oxidation and reduction cycles during oxygen carrier aided combustion (OCAC) operation, as well as ash interaction, affect the magnetic susceptibility of ilmenite particles used as oxygen carriers. Magnetically separated samples of bottom ash collected from Kraftringen's circulating fluidized boiler located in Örtofta (Sweden) were analysed. The samples were part of an OCAC campaign from April 2018, in which waste wood and wood chips were used as fuel.

Particles from the fresh material, the bottom ash, as well as the fractions separated by a magnet - the magnetic fraction (magnetic accept) and the non-magnetic fraction (magnetic reject) collected from different days were morphologically and chemically characterized using SEM-EDS. XRD was used for crystalline compounds identification and XRF was used for the analysis of the bulk composition of the samples. The aforementioned analysis were complemented with magnetic susceptibility measurements of the samples.

The separation of the magnet was found not to be totally effective as artifacts (namely feldspar in the magnetic fraction and inactivated ilmenite in the magnetic reject) were detected in the samples. The results indicate that prolonged residence time of the bed material in the boiler increased the presence of $CaTi_{0.8}Fe_{0.2}O_{2.9}$ enrichments in the ash layer of the particles from the magnetic accept fraction. It was observed that ash compounds do not interfere significantly in the bulk magnetic susceptibility. Magnetic susceptibility increased with longer residence time, where the suggested cause behind it was the possible Fe^{2+} migration towards the surface of ilmenite particles, and its oxidation to magnetic Fe oxides – titanomagnetite and hematite.

The results from the work suggest that the magnetic susceptibility of bed material increases with residence time in the boiler, and so does the ash uptake. Early separation can result in fresh material ending in the magnetic reject fraction. Based on these results, an optimal time window for the extraction, separation, recirculation and/or renewal of the bed material can be defined that will likely result in an increase in separation efficiency of the bed material. Therewith, magnetic susceptibility measurements could be a useful tool in the optimization and decision making regarding this time window.

Acknowledgements

Content

List of Figures

List of Tables

1. Introduction

The industrial revolution was characterized by a series of major technological and industrial advances that led to the development of modern societies. Such period brought several inventions, like the car or the steam engine from Newcomen/Watt, that would change reality in a way that directly affected our present world. However, this period did not only bring a positive impact as it was later discovered that some activities that started during this era also had negative consequences. That is, climate change and global warming, two separate consequences that are related to each other. Climate change refers to the modification of the meteorological patterns of the global climate (i.e. precipitations, temperature etc.) and its cause is not only tied to human activities, whereas global warming refers to an observed increase in the Earth's mean temperature and its cause in the last century is mainly anthropogenic. Global warming is directly a consequence of increased greenhouse gas emissions since the pre-industrial era and other human activities. According to scientists, global warming has played a major role in the climate change events that have been happening since the early 1950s and its effects are devastating. Among the climate change events related to global warming hotter days, rising sea levels, more frequent and intense weather events and both warming and acidification of the oceans can be found. Greenhouse gas emission reduction plays a significant role in mitigating and not aggravating these events [1, 2].

Fossil fuel combustion is the largest contributor to the CO_2 and GHG (Greenhouse Gas) emission towards the atmosphere. Data from the U.S. Energy Information Administration shows that in 2018 CO_2 emissions from fossil fuel combustion for energy were approximately 75% of the total US anthropogenic GHG emissions and 93% of total U.S. anthropogenic emissions [3].

Amidst the COVID-19 pandemic that became worldwide in the year 2020, data shows that the CO_2 emissions worldwide virtually decreased. This decrease was around 7% below 2019 $GtCO_2$ levels according to the data from the Global Carbon Project [4]. Of course, the decrease was not homogeneous for every country and there are complex dynamics behind this fact. However, that decrease is far from enough for accomplishing the goals set in the 2015 Paris Agreement. In fact, a rebound in emissions is expected for the present year 2021 mainly due to the temporary measures taken during the start of the global pandemic. According to a recent study published by Le Quéré et al., these measures did not impact significantly the fossil fuel-based infrastructure [5].

One of the precise objectives of the Paris Agreement issued by the UN (United Nations) and adopted by 197 countries in 2015 to tackle climate change was:

 "Holding the increase in the global average temperature to well below 2°C above pre-industrial levels and pursuing efforts to limit the temperature increase to 1.5°C above pre-industrial levels, recognizing that this would significantly reduce the risks and impacts of climate change" [6].

According to the Berkeley Earth Temperature update report, on January 2021 the global mean temperature was 1.18 ± 0.07 °C above the 1850-1900 average, which is commonly used when referring to a pre-industrial period [7].

In order to fulfil the set goals for temperature limits, it will not be enough with achieving zero CO_2 emissions. It will probably be needed to aim for active removal of CO_2 from the atmosphere, as even if null greenhouse emissions are achieved, the climate would still change due to the inertia effects of the climate system [8].

With the consequences connected to the use of fossil fuels, more and more efforts are being put into trying to find a good alternative to coal, oil and natural gas as fuel. Among the different investigated alternatives, there are renewable energies like solar energy, wind energy, hydropower energy, biomass, etc., that aim for a partial or total fossil fuels replacement.

Biomass is a non-fossil product containing predominantly organic but also inorganic constituents. The vast majority of biomass used today originates from nature, even though small shares come from humans, such as for example wood products. The main organic constituents of wood are lignin, cellulose and hemicellulose, with the presence also of other major or minor organic or inorganic components [9].

Biomass can be categorized in different ways. One useful way of classifying is based on biodiversity groups. Based on that category the biomass can be divided into wood and woody biomass, herbaceous and agricultural biomass, aquatic biomass, animal and human wastes, semibiomass (namely contaminated biomass and industrial wastes like sewage sludge) and their mixtures [10].

Characteristic of biomass is that it has a high energy density and is considered to be CO2-neutral. Thus, it can be used as fuel in conventional heat and power plants acting as a bridge between the existing energy system and the future energy system that would most probably be dominated by solar, wind, hydro energy etc. Furthermore, if oxygen carrier aided combustion (OCAC) of biomass is used in existing thermal power plants a pure CO2 flue gas can be obtained which when captured and stored can result in negative CO_2 emissions. Negative CO2 emissions are what we are looking for to limit the long term increase of global average temperature below 2 °C if compared with what it was in the pre-industrial era [9].

1.1 Fluidized bed technology

The combustion process for heat and power production is usually industrially performed in a grate-fired or a fluidized bed boiler. Fluidized bed boilers tend to be used for larger scale units (>50 MW) than grate-fired boilers (10-100 MW). Fluidized bed boilers can be considered similar to a Continuous Stirred Tank Reactor (CSTR) in the sense that "correct" mixing is promoted in the reactor, whereas a grate-fired boiler would be closer to a Plug Flow Reactor (PFR) as the given fuel goes through a series of different stages (Drying, Pyrolysis, Char burning etc.). In every stage of the process in a grate-fired boiler, O_2 and air need to be fed. In the past, this meant that grate-fired boilers used an excess of O_2 in comparison to the fluidized beds but with computer optimisation this difference has been narrowed to the point that it is almost non-existent [11].

One of the common techniques used in chemical engineering is fluidization and fluidized beds.

Fluidized bed technology consists of the use of a reactor in which small particles referred to as bed material are set in motion by a gas introduced in the reactor. The bed material particles even though solid, after a certain gas flow rate of the introduced gas is reached, begin to behave as a liquid (e.g. they possess a certain "viscosity", the bed follows Archimedes law). By using fluidized bed reactors, the heat transfer is improved, which allows continuous operation. The improved oxygen distribution and the improved heat transfer are the reason why fluidized bed technology is considered a good alternative when using low-cost solid fuels.

Fluidized beds are either bubbling fluidized beds (BFB) or circulating fluidized beds (CFB). In BFB the bed remains in the reactor, in stationary conditions, and in a CFB particles are carried out of the boiler and recovered with a cyclone so that the bed is maintained through external recirculation. CFB operates with a higher gas flow and part of the bed leaves the boiler because

the velocity of the air inside the boiler surpasses a velocity named terminal velocity. The particle size also varies from one type of bed to the other [11].

The bed material used in fluidized bed reactors consists usually of solid particles from an inert material, typically silica sand (with main phase SiO_2), although in some variations of the combustion process, such as CLC (Chemical Looping Combustion) and OCAC (Oxygen Carrier Aided Combustion) the material is substituted partially or totally for a material with oxygen carrier properties. For instance, an inert material in the bed material context is a material that does not react in a preferred manner. That does not mean that an inert material cannot become activated due to ash interactions, for example, or vice versa. An active material can also be deactivated and become inert towards a preferred behaviour.

With regular inert bed material, drying and devolatilization of the fuel take place close to the fuel inlet, causing oxygen-poor regions there and oxygen rich regions at the air inlet. These regions create local hotspots and provoke a loss of combustion efficiency. With the increased presence of hot and cold spots, a poor contact between the fuel and O_2 is reached which leads to incomplete combustion and the release of unburned species [11].

1.2 Oxygen Carriers

Oxygen carrier (OC) bed material improves the oxygen distribution (consequently reducing incomplete combustions and the rate of NO_x released) and decreases temperature gradients, reducing the risk for hotspots.

Oxygen carriers were already used in the mid-20th century for syngas and CO_2 production.

An oxygen carrier is a material meant for transporting oxygen from an oxygen-rich region to an oxygen-poor one, thus making it possible to evenly oxidize the fuel and thereby to accomplish a complete combustion or a more complete partial oxidation towards the formation of syngas. Usually, oxygen carriers are based on transition metal oxides, especially oxides of nickel, copper, manganese or iron. Out of all the transition metal oxides, Mn and Fe oxides are generally considered to be benign for the environment. Pure oxides, combinations of transition metal oxides or ores containing transition metal oxides can be used as oxygen carriers. Pure oxides can be combined with an inert binder. A binder serves usually as a porous support that provides a bigger surface area and can also increase mechanical resistance. Common examples of oxygen carriers are ilmenite ($FeTiO_3$), Mn ores, Fe ores, etc [11].

Among the properties an oxygen carrier should possess it can be highlighted that an oxygen carrier should be reactive with both oxygen and fuel, stable, environmentally friendly, show good fluidization properties, have high enough oxygen transport capacity and last but not least it has to be economically viable and available. It is also important that the particle has a long lifetime that is determined by the oxygen transfer capability of the carrier as well as its chemical resistance to unfavourable interactions with biomass ashes and mechanical resistance to physical stress [11].

The oxygen carrier concept, i.e. using oxygen carriers instead of inert bed, along with fluidized bed technology is used in two types of processes that have had a big influence in the field of biomass combustion during almost the last two decades – Chemical Looping Combustion (CLC) and Oxygen Carried Aided Combustion (OCAC).

Chemical Looping Combustion (CLC) represents a technique that separates the combustion process in two reactors, and thereby allows to obtain a non-diluted by N_2 CO_2 gas stream. That stream can be later on compressed and stored with a lower energy penalty than in conventional

combustion processes. The two reactors, the Air Reactor and the Fuel Reactor, are fluidized bed reactors where oxygen carriers are used as bed materials.

With some OCs, a Chemical-Looping with Oxygen Uncoupling (CLOU) mechanism is also present along with regular CLC. CLOU is based on the same principle as CLC but there is an O_2 release from the oxygen carrier to the gas phase. The O_2 released goes on to react with the fuel, resulting in faster oxidation than with the regular heterogeneous reaction between the fuel and the solid OC. However, ilmenite is considered a non-CLOU OC so the CLOU process will not be further discussed in this report [12].

In OCAC the OC is not strictly subject to an oxidizing or reducing atmosphere like in CLC, as it is used to replace the bed material of a conventional CFB. Thus, the oxidation and the reduction do not take place in separate reactors and the boiler presents milder local reducing and oxidizing environments compared to CLC. That is why the OC has to be reactive in continuously varying oxidizing/reducing conditions.

An oxygen carrier can either be synthetically manufactured or it can be extracted from a natural ore or from an industrial waste stream. A natural oxygen carrier is found directly in the nature and does not require extensive treatment apart from crushing or sieving. Manufactured materials are based on natural materials that are subjected to treatments like, for example, incorporation of additives and heat treatment among others. Manufactured or synthetic materials tend to be more expensive than natural/waste materials. Natural and waste stream materials are increasing in importance for use as OCs. This can be confirmed by the data published by Lyngfelt et al. [12], that shows that there was a 68% increase in the operation time of natural ores and waste materials as OCs during the years 2014-2018. That means that at the end of 2018 the share of use of these OCs had doubled if compared to the share in 2014. This research takes into account a total of 11338 hours of operation in total spread over 212 publications [12]. Ilmenite is one of the most widely studied and used OCs with solid fuels and it is indeed the most recurrent OC inside the natural/waste category [9, 11].

In OCAC, the OC can be deactivated and part of the material can be lost as fines due to attrition, which means that part of the bed needs to be regenerated either with new bed material or recirculated bed material that has undergone a treatment or separation. This leads to generating waste material flows and increases the overall cost for the process if expensive OC materials are used as bed material. That is why the target for OC research and operation are already existing low-cost materials available in large quantities. Ilmenite fulfils the requirements of a good OC and that justifies the increase in research studies involving this ore during recent years [11].

1.3 Ilmenite

Ilmenite is a naturally occurring mineral composed of the ilmenite phase $FeTiO_3$ which can be oxidized to Fe_2TiO_5 (pseudobrookite). Ilmenite transports oxygen by changing the degree of oxidation of iron from 3+, as in pseudobrookite, to 2+, as it is in ilmenite. While undergoing this change it oxidizes the fuel in the reactor. Because of this redox reaction, Fe is considered to be the active oxygen transferring element while Ti is not active in the oxygen transfer [12, 9].

Ilmenite exists in the form of sand or rock ilmenite. Both share the same chemical composition (the main phase is $FeTiO_3$) and the main difference is the particle size and morphology. Sand ilmenite particles have smooth rounded shapes due to being exposed to erosion, attrition and other kinds of natural weathering. Instead, rock ilmenite particles have sharp edges because the rock comes from the direct mining and crushing of the ore. Sand ilmenite sometimes shows a higher content of TiO_2 due to natural oxidation and dissolution of Fe during weathering [15].

Usually, it is more common to find rock ilmenite than sand ilmenite in OC applications because it often has a higher oxygen transferring capacity. That comes from the fact that it is common to find more Fe in the rock ilmenite particles than in the sand counterpart [11].

Fuels also take a huge part in how the combustion process with an OC develops. Among all types of fuel, gaseous fuels are the most convenient regarding their handling and homogeneity. These types of fuels can react directly with the OC in a fast gas-solid reaction and can also act as a fluidizing agent. One example of gaseous fuels is syngas. For the solid fuels, in order to react with the OC, the volatile part of the solid fuel has to be released. The reaction that takes place is also a gas-solid reaction but the additional step of volatilization adds complexity to the process. The remaining solid chars go through a similar process as the solid fuels that need to be combusted [11].

1.4 Biomass ash

During the combustion of the fuel, bed material and flue gases are not the only species present in the reactor.

Ashes are the remaining fractions from the fuel after combustion. Biomass ash is a complex heterogeneous mixture of mainly types of inorganic matter but also to a lesser degree organic matter. In the boiler there are two types of ashes - fly and bottom ashes.

Fly ashes consist of the fine particulates left after fuel conversion that leave from the upper part of the boiler entrained by the flue gases. They are usually separated by the cyclone and the filter and can provoke corrosion and fouling if they get deposited on the heat equipment that is part of the downstream processing of the flue gases [11].

Bottom ashes consist of bed material and ash components that stay in the dense part of the bed and they are the main contributors to bed agglomeration and defluidization.

The main bottom ash components are silicon, alkali (mostly K and Na) and alkaline earth (mostly Ca and Mg) in the form of oxides, carbonates, chlorides, hydroxides and sulphates. Ashes can also incorporate elements such as aluminium, titanium, sulphur or phosphorus. The composition of biomass ashes depends on three factors: the type of biomass and conditions in which the biomass resource is obtained and stored, the conditions in which the combustion takes place and both the transport and storage conditions of the ashes. It is widely accepted that wood and woody biomass yields the minimum amount of ashes compared to the other groups, being animal and waste flows like municipal solid waste the resources that have a higher ash yield (it can be up to 50-70%) [10].

When referring to biomass or its ashes, elemental concentrations are a valuable measure of the composition of a sample. Depending on the concentration of a certain element, it can be classified as a major (>1%), minor (1-0.1%) and trace (<0.1%) element in the sample. Following this classification, typically the major elements in biomass are C>O>H>N>Ca>K and the minor elements are Si>Mg>Al>S>Fe>P>Cl>Na. Of course, the ash composition varies depending on the source of the biomass but that classification is generally accepted, along with the inclusion of Mn and Ti as minor elements. The composition of the biomass ashes varies depending on the type of biomass that was used for combustion but it has been found that wood and woody biomass shows a low concentration of Cl, K, Na and S while being rich in Ca [10].

Ilmenite reacts with the main ash elements, K and Ca, forming new compounds either while diffusing into the bed material particles (such as e.g. KTi_8O_{16}) or while staying attached to the particle surface (such as e.g. $Ca(Ti_{0.7}Fe_{0.3})O_{2.5}$) [16]. The formation of these compounds can lead

5

to K capture which prevents the formation of gaseous K compounds that can corrode the heat exchanger equipment present in the downstream processing of the flue gases. That type of corrosion leads to extensive maintenance costs. Therefore, it translates into a great loss of both production and money. The mechanism of reaction to form the listed titanate compounds is hard to assess and remains unclear.

1.5 Reactions

The main role of the OC in an OCAC application is to transfer oxygen from the oxygen rich sites to the oxygen lean sites of the reactor. The chemical mechanism behind that is based on redox reactions between the oxygen carrier and its environment.

1.5.1 Ilmenite reactions with organic constituents from the fuel

The OC must be first oxidized in an oxygen rich location (e.g. near the air inlet of the combustion chamber) by air:

$$Me_xO_{y-1} + \frac{1}{2}O_2 \rightarrow Me_xO_y \qquad (R1)$$

In the case of ilmenite, the oxidation occurs following the next reaction:

$$2FeO \cdot TiO_2(s) + \frac{1}{2}O_2(g) \rightarrow Fe_2O_3 \cdot TiO_2(s) \qquad (R2)$$
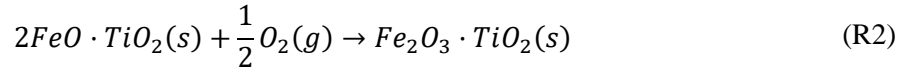
And then, the OC is reduced at an oxygen lean location (e.g. near the fuel inlet).

The fuel will react to form volatile compounds and char (these last organic compounds are also converted to CO) [11, 14].

$$Biomass\ (C_aH_bO_c) \rightarrow volatiles\ (C_iH_j) + char\ (C_xH_yO_z) \qquad (R3)$$

$$char(s) + H_2O(g) \rightarrow H_2(g) + CO(g) \qquad (R4)$$

$$char(s) + CO_2(g) \rightarrow 2CO(g) \qquad (R5)$$
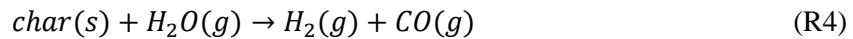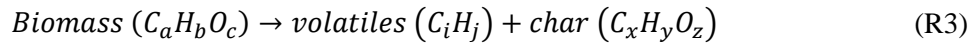
Volatiles are in the form of nC_iH_j gaseous hydrocarbons and along with CO they react with the OC in a redox reaction that yields CO_2. During that reaction the OC is reduced.

$$H_2(g) + CO(g) + nC_iH_j(g) + Me_xO_y(s) \rightarrow CO_2(g) + H_2O(g) + Me_xO_{y-1}(s) \qquad (R6)$$
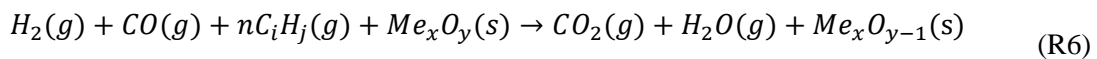
During this reaction the OC reacts with the volatilized hydrocarbons. However, inside the reactor there is also CO that comes from the gasification of volatiles and chars, and it can also yield CO_2 when oxidized. Taking ilmenite as the OC of choice, the reaction should be the following.

$$xFe_2O_3 \cdot TiO_2(s) + aCO(g) + bC_iH_j(g) \rightarrow 2xFeO \cdot TiO_2(s) + cCO_2(g) + dH_2O(g) \quad \text{(R7)}$$
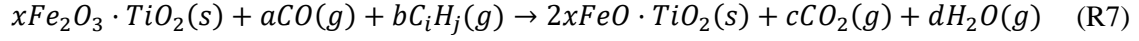
Where pseudobrookite formed in the oxygen rich sections is reduced to ilmenite again [14].

During the oxidation of ilmenite, multiple studies have found that an Fe_2O_3 layer is formed on the surface of the particles and that the oxidizing conditions promote the separation between Fe and Ti inside ilmenite particles [18, 19]. This Fe oxide layer is formed as a result of Fe^{2+} and Ti^{4+} diffusion towards regions with high oxygen partial pressures, such as the surface of the particle. While Fe^{2+} and Ti^{4+} are diffusing towards the surface of the particle, oxygen molecules are diffusing inside the particles. According to Knutsson et al. [18], Fe^{2+} diffuses faster in $FeTiO_3$ than Ti^{4+}. When reaching the surface, Fe^{2+} ions are oxidized to Fe^{3+} as in Fe_2O_3 and that is how the hematite layer is developed. D. Rao et al. [19] state that under 770 degrees Fe_2O_3 is formed on the surface of the particle. Since O_2 has to diffuse through Fe_2O_3 further reaction occurs at the Fe_2O_3-$FeTiO_3$ interface. Then, between 770 degrees and 900 degrees $Fe_2Ti_3O_9$ (pseudorutile) is formed and iron diffuses through it to the available grain boundaries, cracks or the surface, where the oxygen partial pressure is higher [19]. Since during oxidation at even higher temperatures pseudobrookite (Fe_2TiO_5) is also formed, to present Fe-Ti segregation the mobility of the Fe cations through the structure has to be high, due to the fact that the Fe:Ti ratio is higher for Fe_2TiO_5 than for $FeTiO_3$. Other than the suggested mechanism, it is possible to find other mechanisms for this Fe-Ti segregation in the literature as it has been described in multiple ways.

The following reaction is a suggested reaction for the formation of pseudorutile from ilmenite:

$$2FeO \cdot TiO_2(s) + TiO_2(s) + \frac{1}{2}O_2(g) \rightarrow Fe_2Ti_3O_9(s) \quad \text{(R8)}$$
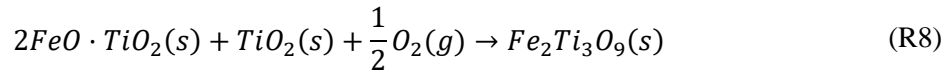
The compound formed is pseudorutile. Pseudorutile, according to Fu et al. [20], has a slightly lower lattice density than ilmenite which could facilitate the migration of Fe^{2+} through the structure, as observed by Corcoran et al. [21]. This allows more formation of hematite (Fe_2O_3) and the migration of Fe content outwards the particle [21]. Recent studies state that it is precisely this Fe migration outwards the cause of the phase separation between Fe_2O_3 (outer part of the particle) and TiO_2 (inner part of the particle) [16].

The Fe migration towards the surface improves contact with air. That effect, combined with the fact that Fe is the active element in oxygen transferring leads to an increase in oxygen transferring capacity. However, attrition is happening with or without Fe on the surface. The problem with that is that while Fe migrates towards the surface, Fe attrition also increases, reducing the OC ability as the active element is lost. This phenomenon reduces the overall lifetime of the OC particles. Fe migration also increases the porosity of the particles, increasing the particle/air reaction surface. That porosity increase is only correlated with an increase in OC ability in the cases where attrition is not dominant and there is still enough Fe in the structure [11].

Fe tends to migrate to areas with a high oxygen partial pressure. In the case of sand ilmenite, this migration tends to be more intense towards certain cracks and cavities of the particle, where structural defects act as passages for oxygen diffusion. However, this is not the expected behaviour for rock ilmenite. Since fewer cavities are formed in these particles it is more common to see Fe migrating towards the surface, as it is the nearest location with a considerable oxygen potential [11].

Another possible scenario for the observed Fe-layer at the outermost surface is that a formed outer ash layer (the formation of this layer will be further explained later on) can be worn off due to attrition and as a result, the Fe layer is present on the surface. An example of this has been observed in research carried out by Staničić et al. [22].

1.5.2 Ilmenite reactions with inorganic constituents from the fuel (ashes)

Some of the most important reactions between ilmenite and ash compounds are the ones that form potassium titanates inside the core of the OC particles (ilmenite particles) due to potassium diffusion inwards. This reaction happens due to interaction of the TiO_2 core (left after the Fe diffusion outwards in oxidation conditions that has been explained previously) with potassium-based salts or other compounds such as potassium oxides. For instance, KCl has been chosen as the potassium salt for the suggested reaction but other ones could have been chosen too.

$$8TiO_2(s) + KCl(s) \rightarrow KTi_8O_{16}(s) + \frac{1}{2}Cl_2(g) \qquad \text{(R9)}$$
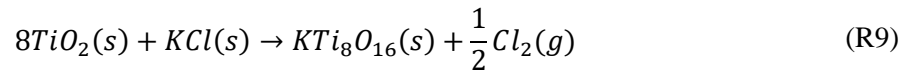
When the K compounds in the combustion chamber (e.g. KCl) are not taken up by an additive they can leave the combustion chamber with the flue gases. Once released, they can be harmful to the heat exchanging equipment so it is an advantage if K is taken up by the OC. Thus, the ongoing research focusing on how to make ilmenite absorb more K and the limits of that process is beneficial for preventing corrosion [14].

In a similar interaction, Ca compounds can be adhered to the surface of the structure of the ilmenite particle where reaction takes place and Ca^{2+} is incorporated into the titanate structure by reacting with TiO_2 to form $CaTiO_3$ [16]. The following suggested reaction describes the formation of $CaTiO_3$ starting from CaO.

$$CaO(s) + TiO_2(s) \rightarrow CaTiO_3(s) \qquad \text{(R10)}$$
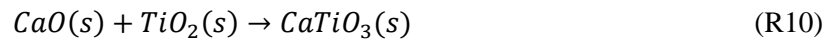
1.6 Alkali uptake and consequences of boiler operation with OC

Several studies have documented how this theoretical set of reactions affect the activity, the morphology and mechanical stability of the ilmenite particles when acting as bed material and the chemical reactions that ilmenite undergoes with the main ash compounds [12, 13, 16].

According to published data, when exposed to combustion conditions, Fe migrates towards the surface of the particle, forming an iron-rich layer. This layer is either a uniform layer or it appears as iron-rich clusters or islands at locations where the oxygen partial pressure is higher. For the same combustion conditions, Corcoran et al. [16], found that the potassium and calcium compounds of the ashes react with the ilmenite particle forming new compounds. On one hand,

potassium compounds form what is thought to be KTi_8O_{16}, a result of K diffusing into the particle core and reacting with TiO_2. On the other hand, a Ca-rich double layer is formed around the Fe-enriched layer that can be found on the particle. This double layer consists of an outer layer that accumulates on the surface of the particle and an inner layer that presents a more homogeneous composition than the outer one. The outer Ca-rich layer incorporates other ash compounds (such as Si and P). The inner layer is the result of the formation of a new compound, $Ca(Ti_{0.7}Fe_{0.3})O_{2.5}$ (or $CaTiO_3$ in sand ilmenite), which is formed when Ca^{2+} migrates inside the particle and reacts with the inner ilmenite structure. The formation of this Ca double layer is presented in a Corcoran et al. research [16].

In the study of Corcoran et al. [16], ilmenite was tested in the Chalmers CFB research boiler as an oxygen carrier in the bed reactor. The fuel used was mainly wood chips, the mean operation temperature was 850 °C and the test went on for a span of 6 weeks. After that period, the particles with a higher residence time were chosen due to theoretically being the most representative of the degree of interaction with ash compounds [16].

To study agglomeration and the mechanical stability of the particles, SEM-EDX and XRD analysis were performed on these particles. A shift towards larger particle diameters and a reduction in the number of the finest particles was found after the experiment. The first effect observed after the experiment could be caused by layer formation, an increase in the particle's porosity (and thereby increase of the volume of the particles) and the incorporation of ash compounds. Another possibility could have been the agglomeration of particles, although agglomeration was not visually observed. The reduction of the number of fine particles could be explained by the entraining of the finest particles in the flue gases.

When it comes to the morphology of the particles, it was observed that sand ilmenite particles had increased the number of cavities and had undergone cluster and cracks formation. It was also noted that bright spots appeared on the particles' surfaces. These spots were rich in iron while the remaining darker spots were similar to the composition of the initial fresh ilmenite. Iron-rich clusters tended to appear on the surface, often close to cracks. The theory that explains this fact is that the cavities are short passages for oxygen diffusion and that increases the oxygen potential locally [16].

When no cavities were formed (at early stages of exposure) EDS revealed that a layer had formed. That layer had a similar composition to that of the bright spots on the surface (rich in iron). The inner part of the particles had also a similar composition to that of the initial fresh ilmenite. Smoother parts of the surface were observed to be rich in magnesium and calcium and it was noted that these areas had become poorer in iron and titanium compared to fresh ilmenite [16].
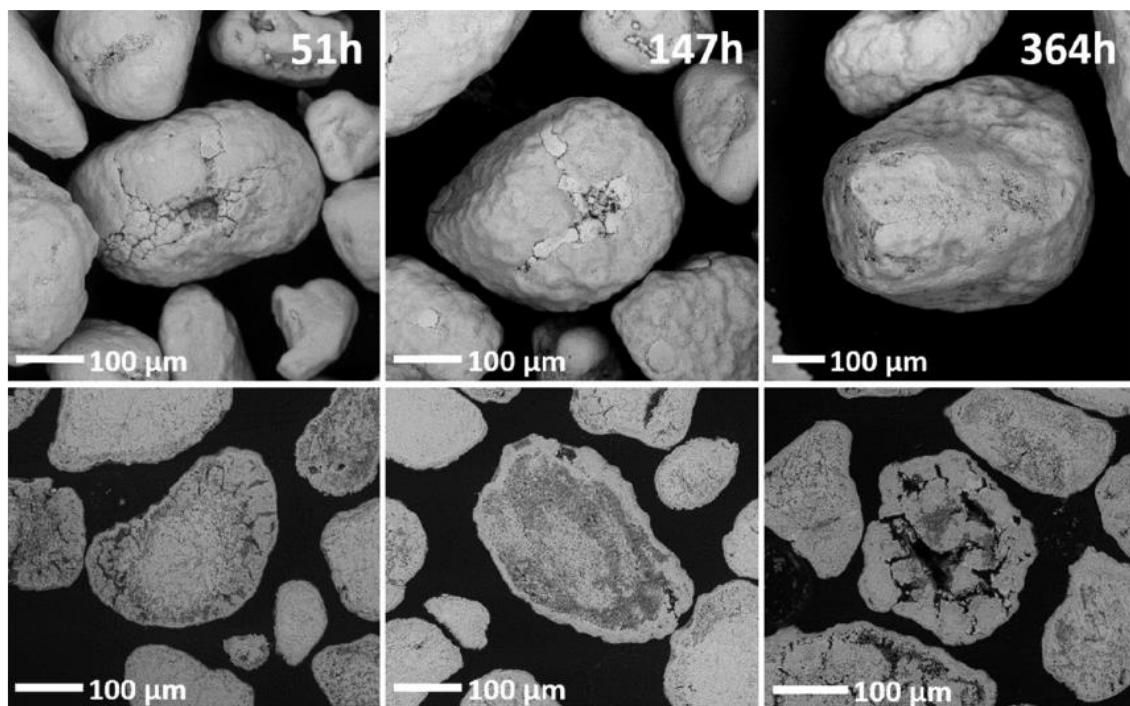
Figure 1. Backscattered Electron Micrographs of used (51, 147 and 364 h) of ilmenite particles used as bed material. Fe rich smooth clusters can be seen in the 147h top row overview while the Fe rich layer can be seen in the 147h bottom row cross-section of the particle [16]**.**

With what had been observed, some conclusions were drawn regarding the kinetics of the ash – ilmenite interactions and the diffusion of the layers and their thickness.

Corcoran et al. [16] observed that an outer Ca-rich layer is formed on the surface of the particle, and it accumulates with time, thereby becoming thicker. The concentration of Ca in the layer does not change significantly but the thickness of the layer does. Also, Ca^{2+} migrates inwards through the titanate structure, resulting in an inner layer that can be distinguished from the outer layer.

Three hypotheses were formulated to explain the formation of the inner Ca-enriched layer: 1) Ca is deposited from the ash on the surface while the particle grows in diameter, remaining "locked" inside the ash layer; 2) Ca is deposited from the ash and migrates inwards the particle and 3) Ca existing in the fresh ilmenite migrates outwards. The expected main source of Ca is the ash because of the thickness of the surface layer. This expectation does not align well with the third hypothesis. While the migration inwards could explain the presence of the internal layers, it does not align well with the fact that P and Si were found at the external parts of the Ca layer. These elements (P and Si) would migrate inwards at different rates. This last fact was not proven due to not being the main purpose of the investigation [16].

P and Si compounds are not originally found on fresh ilmenite particles. Thus, the finding of P and Si compounds in the layer suggested that both elements were deposited as ash components directly outside of the particle.

Finally, it was suggested a mechanism that combines hypothesis 1) and hypothesis 2). In this mechanism, Ca compounds form a layer outside of the particle that grows outwards and also Ca migrates inwards, reacting with TiO_2 from the internal structure of the particles and forming $CaTiO_3$ or similar Ca-titanates [16].
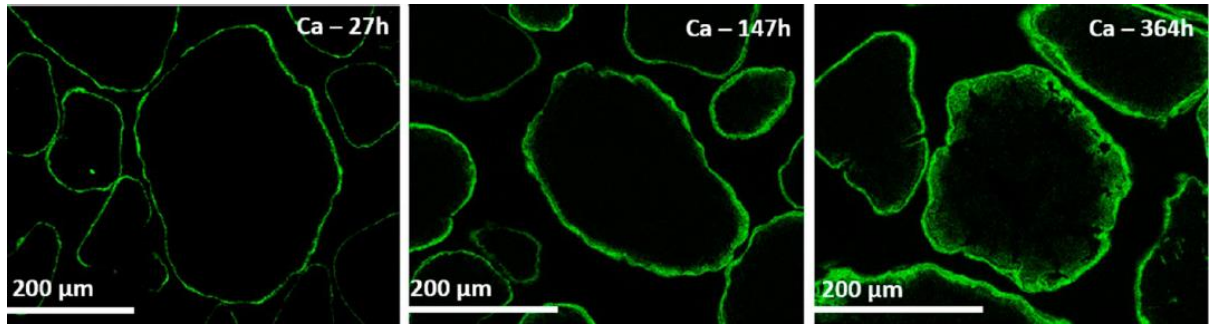
Figure 2. Illustration of the growth of the Ca layer in ilmenite particles and its migration inwards after several operation hours (27 h, 147 h and 364 h from left to right respectively). Images obtained as Ca EDS-intensity maps [16]**.**

A similar analysis for K showed that it was not present in the Ca surface layer. However, it also formed outside of the particle and migrated inwards, until reaching the limit of 2% in atomic composition in the particle. That limit was the K uptake limitation in the exact conditions of that experiment. According to experimental results, the particle was considered to be rich in potassium (and therefore having reached the limit) after 83 hours of operation.
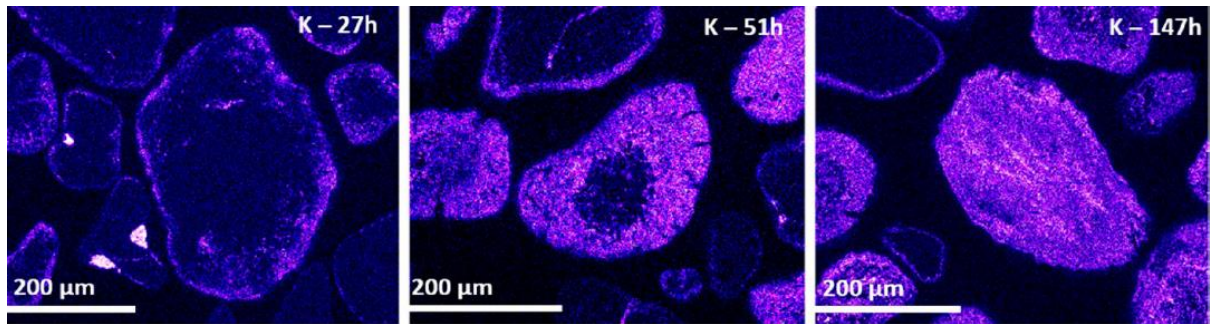
Figure 3. Illustration of the migration of K in ilmenite particles and its migration inwards after several operation hours (27 h, 51 h and 147 h from left to right respectively). Images obtained as K EDS-intensity maps [16]**.**

Although it was not the goal of the research, it was suggested that cracks could be spots for migration inwards of Ca and K compounds.

The main difference between the Ca and the K compounds formed on the surface is that Ca compounds tend to accumulate on the surface and then migrate inwards with time, while K compounds do not only accumulate on the surface. It is regarded that the migration of K inwards is faster than Ca migration, although the migration of K is promoted by the presence of Ca on the surface [16]. Both K and Ca react with TiO_2 to form $K_2Ti_3O_7$/ $K_2Ti_6O_{13}$ and $CaTiO_3$ but this last compound is the most stable among the three. This stability reduces the free TiO_2 on the surface and promotes the migration of K inwards [16].

Another study by Corcoran et al. [21] also characterized the shift in composition from ilmenite when in contact with bottom ashes during OCAC operation. In that study, some samples were analysed before, during and after OCAC operation with bed material replacement with ilmenite. First, 20% of the silica sand was replaced with ilmenite and after two days of operation, approximately 40% of the bed material was ilmenite. Elemental analysis of the samples obtained show how the Fe weight % diminishes with time while Ti weight % stays quite constant and Ca, K, Si, P and Mn weight % increase [21].

Another interesting view is the global standpoint regarding what happens to the weight of ilmenite during operation, and how that can be reflected by the observed differences in weight before and after its use as bed material. From this standpoint, Hildor et al. [14], observed with the help of TGA that when an ilmenite sample was oxidated it gained weight whereas in reducing conditions part of the weight was lost. In fact, the rate at which weight was gained in oxidating condition was faster than the rate of losing weight in reducing conditions [14].

It is expected, then, to see a weight gain when operating with ilmenite as the OC and bed material at the same time. This weight gain, though, is expected to be slowed down due to the great loss of oxygen and salts such as sulphur salts and KOH with the flue gases. The amount of weight loss expected varies depending on the reducing conditions of the reactor and the dryness of the internal environment. Regarding strictly the bed material and considering the inlet and outlet streams of the boiler, it is expected to observe a weight gain due to ash layer build-up.

Especially in the presence of steam, KOH is formed and evaporated, thus provoking fewer interactions between ash K compounds and ilmenite particles. Under these conditions, then, it is expected less K % in the sample than in absence of moisture. Regarding S compounds that can be transferred onto the ilmenite, a weight loss was expected under wet and dry conditions due to the vaporization as SO_2 or H_2S [14].

1.7 Magnetic separation

Since in the middle of the 18th century Michael Faraday discovered that a substance in the way of a magnetic field increases or decreases (to some extent) the flux density of the magnetic field (B) when passing through it, a broad range of applications that stem from this phenomenon have been discovered and applied.

Magnetic separation is one of those applications. It is based in the fact that materials can be separated based on their different magnetic properties. The first widely extended commercial application for the process came in the late 1860s, when it was introduced in the separation of iron from brass [23]. This process, however, has been used in many industries since then. Some examples are the magnetic traps from food industry that exclude metal foreign bodies that could be a food safety hazard from certain food products, the magnetic separators used for waste management in recycling centres or its use in wastewater treatment in steel industry and in power plants [24].

There is a wide variety of magnetic separators in the different industries that require this technique, but the most common separators are the following ones:

- Magnetic pulleys: Elongated cylinders supported by a shaft that constitutes the head pulley for conveyors that transport material in the plant. The pulleys have magnets installed or attached to them so that they provide a constant magnetic field around the whole circumference.
- Suspended magnets: Permanent magnets or electromagnets purposely suspended over a conveyor belt or a feeder that transports material.
- Magnetic drums: A magnet assembly is built inside a rotating drum cylinder that draws the magnetic particles onto its surface and carries them outside of the range of influence of the magnet.
- Plate magnets: Magnets designed in the form of plates are placed down a chute from which material falls. The magnetically separated material attached to the plate has to be removed periodically from its surface.

- Grate magnets: Several magnetic rods or tubes are disposed inside a support frame through which the material is supposed to flow (the material is usually free falling towards the magnet) [23].
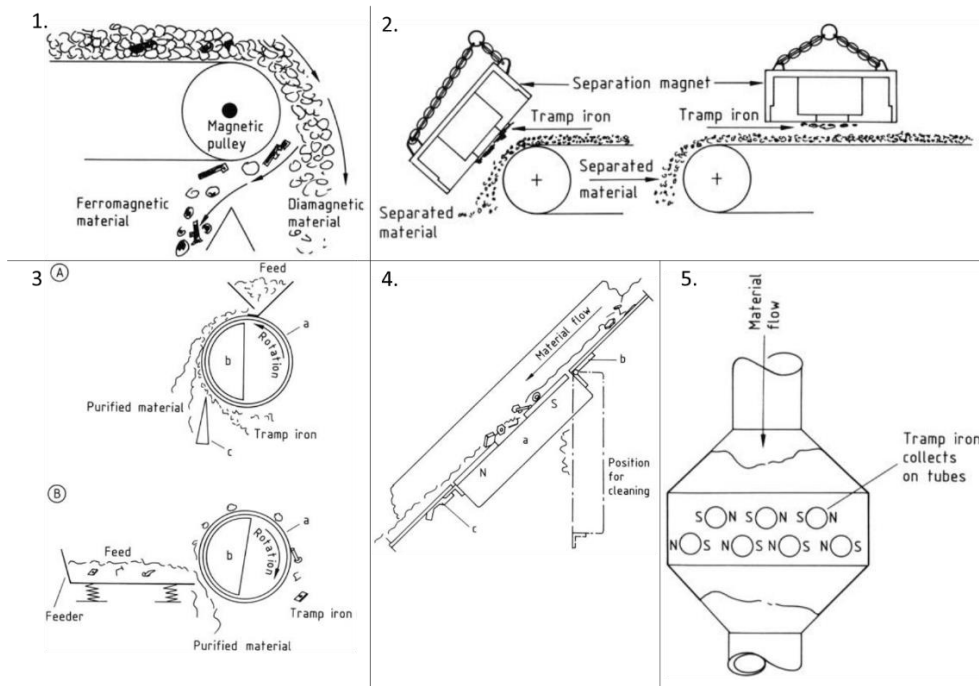
Figure 4. Illustration of conventional industrial magnetic separators: 1. Magnetic pulley; 2. Suspended magnets; 3. Magnetic drums; 4. Plate magnet; 5. Grate magnets. Arranged from the original source [23]**.**

Magnetic pulleys or belt separators are recurrent in many industries because these magnets are easy to install, have a low initial cost and a low cost of operation (if the magnets are permanent, such as rare earth ones), and are able to accomplish continuous and automatic removal of magnetic materials. However, these separators are still a highly empirical technology. The aim of the separation is to obtain the right quality of the concentrate with the right recovery, and that is fixed by the user with an adjustable non-magnetic splitter [25].

The driving force in the separation is the magnetic force (F_m), that competes with external forces such as gravitational force (F_g), the hydrodynamic drag force (F_d), fraction force (F_f) and inertia (F_i), depending on the type of the operation. Whatever the dynamic system is for the process, it needs to be made sure that the magnetic force of the magnetic materials that need to be recovered is higher than the competing forces. Else, it will fall with the non-magnetic material. In order to do that, several things need to be adjusted, such as the pulley revolutions in a magnetic pulley, as overly high revolutions could cause an unwanted centrifugal effect that diminishes the performance of the separator. Particle size also has a lot to do with the degree of recovery achieved. Usually, the magnetic pulleys are used in systems that have particles of a wide variety of diameters and that is why the splitter between magnetic fraction and non-magnetic fraction is adjustable [20, 21].

In industrial-scale boilers such as the Kraftringen's 115 MW$_{th}$ CFB boiler located in Örtofta, it is common to extract samples of the bed material and magnetically separate them to introduce the magnetic fraction again in the boiler. This is handled by a roll belt magnet located around two cylinders that rotate continuously to displace the entities placed on the belt. The magnetic separator acts as a conveyor belt for the samples until they approach one of the extremes, where

a rare earth magnet separates the two possible parts of the sample based on their magnetic susceptibility. The fraction of the sample that is magnetic is often called magnetic fraction or magnetic accept while the fraction that is not magnetic is often referred to as non-magnetic fraction or magnetic reject. The cylinder magnet keeps the magnetic parts of the sample attached while releasing the non-magnetic fraction with a parabolic trajectory directly onto a container where the magnetic reject is kept. The magnetic fraction rolls all over to the bottom part of the belt while being attached to it until the magnetization is not strong enough to keep the fraction attached to the belt and it falls directly into a container where the magnetic accept is kept [11].
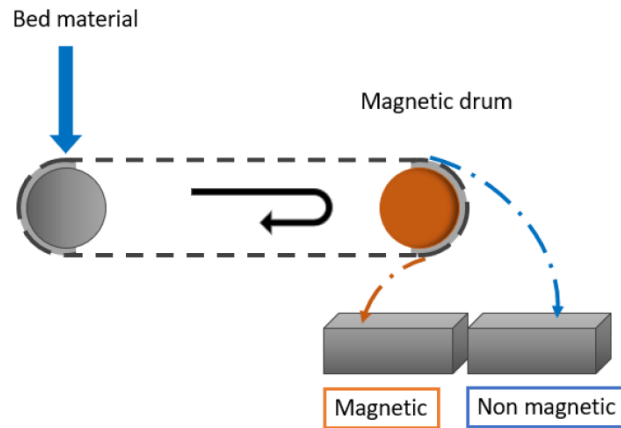
Figure 5. Illustration of the described magnetic separation used in an industrial-scaled plant [11]**.**

The purpose of this separation is to recover the fraction of active ilmenite that can be recycled from the ashes and other products that should be removed from the boiler. The system is promising and allows for bed material recovery, where for example, in the Kraftringen combustor the separation system has a capacity of up to 700 kg/h of sample and up to 8 times recovery of the bed, according to communication with industrial partner [11].

Magnetic separation combined with recirculation of bed material in the OCAC process is indeed a way of optimizing the usage rate of ilmenite while reducing the material streams (fresh material and waste) of the bed material that needs to be put in a landfill and the overall cost of the process.

Of course, the used bed material will be separated based on the compounds present in the particles. It depends on whether they have magnetic properties and which type of magnetism do they show. As a measuring and comparing property for that, magnetic susceptibility can be used.

To define magnetic susceptibility, two other field properties must be defined:

Magnetization (M): It is the vector field that expresses information about the density of permanent or induced magnetic dipole moments in a sample. It can also be defined as the quantification of magnetic dipolar moments per unit of volume. These magnetic dipoles can be generated through three sources:

- The spin of the electrons of the atoms.
- The orbital angular momentum of the electrons about the nucleus.
- The change in orbital moment induced by a certain applied magnetic field. This source is strictly tied with diamagnetism and Lenz's law for electromagnetic fields [27].

Intensity of the applied magnetic field (H): The intensity of the magnetic field is a measure of how strong or weak the external magnetic field is (independent of a certain material magnetic

response). It is strongly related to the magnetic flux density or magnetic induction (B) by the following equation:

$$H = \frac{B}{\mu} \tag{E1}$$

Where μ is the permeability of the medium or the material through which H passes [28].

Magnetic susceptibility (χ) is the quotient between the magnetization of the sample M and the intensity of an applied magnetic field H:

$$\chi = \frac{M}{H} \tag{E2}$$

Magnetic susceptibility gives an idea of the "magnetizability" of the sample. That is, how easy it is to provoke a certain magnetic moment based on the strength of the magnetic field applied.

Magnetization (M) and intensity of the applied magnetic field (H) have the same units (Amperes per meter or A/m in SI units). Therefore, magnetic susceptibility is dimensionless. What is usually referred to as the non-dimensional magnetic susceptibility is specifically called volume specific magnetic susceptibility.

The permeability of the vacuum (μ_0) is a property that can be related to the permeability (μ) and the magnetic susceptibility thanks to Equation 3:

$$\mu = \mu_0(1 + \chi) \tag{E3}$$

Materials can be classified into five categories according to their magnetic behaviour:

1. Ferromagnetism: The magnetic moments of the sample are ordered in one direction and thus the magnetic susceptibility of the material is high. This type of materials is hardly ever found present in the nature.
2. Ferrimagnetism: The magnetic moments of the material are ordered and aligned but instead of being ordered in one direction they have two unequally opposing moments. That reduces the magnetic susceptibility when compared to ferromagnetic materials. Ferrimagnetic materials are also more common in the nature than ferromagnetic materials.
3. Antiferromagnetism: Similar to ferrimagnetism in the sense that for antiferromagnetic materials the magnetic forces also oppose but, in this case, they virtually cancel each other completely, and only when a magnetic field is or has been present (they have a remanent magnetization) they can be magnetized.
4. Paramagnetism: Paramagnetic materials have their magnetic moments organized randomly without absence of magnetic field and thus their magnetic susceptibility is weak. They can only be magnetized in the presence of a magnetic field.
5. Diamagnetism: This type of materials shows a negative magnetic moment that appears due to a variation in the magnetic field flux. It is a universal property from electrons that follows Lenz law.

Lenz law states that when a change in magnetic flux appears close to a conductor in a circuit (in this case an electron following an orbit can be understood as one), a current will be induced in the circuit in order to create a magnetic field that opposes the external change in magnetic field.

In order to be considered a diamagnetic material, it does not have to show any of the previous 4 behaviours because otherwise they will predominate. Thus, a diamagnetic material is a material that strictly shows zero net magnetic moment in the absence of a magnetic field and it normally has negative magnetic susceptibilities due to having a negative magnetization that weakens the flux density [29].

When considering a material that contains chemical phases that may be classified in different categories, the magnetic susceptibility is more difficult to assess as a smaller amount of the more magnetic material can have a major effect on the value of the magnetic susceptibility of the bulk blend. That is because the difference in magnetic susceptibility between different types of magnetism can be of several orders of magnitude.

Another concept needs to be introduced when considering the magnetic properties of materials, and that is the Curie/Neél temperature.

As temperature rises, thermal agitation results in magnetic moments from an antiferromagnetic material no longer cancelling each other and then an increase in magnetic susceptibility and a weak magnetization is produced. At a temperature named Neél temperature (T_N) the atomic moments become paramagnetically disordered and the material starts behaving de facto as a paramagnetic material. An antiferromagnetic material behaves as a paramagnetic material above T_N.

The same thing happens for ferromagnetic and ferrimagnetic materials. Above a certain temperature named Curie temperature (T_C) they start behaving as paramagnetic substances [30].

1.8 Fe magnetic species

Some elements that form species that can have magnetic properties are Fe, Ni, Co, Gd, Tb and others. Among all of these, the most common one expected in ilmenite samples is Fe. Mn can also form some antiferromagnetic phases but the amount expected in the samples is considerably lower than that of Fe.

Therefore, the main focus regarding magnetic compounds will be placed in Fe magnetic phases. The following magnetic phases may be relevant in the report:

- Fe_2O_3: Commonly known as hematite, it is one of the most common Fe oxides present in the nature as α-Fe_2O_3. The less abundant β-Fe_2O_3 phase is known as maghemite. In the pure form and at room temperature, hematite is antiferromagnetic. It has a Neél temperature of approximately 675 °C and it shows paramagnetism over that temperature [30].
- Fe_3O_4: Commonly known as magnetite, it is a ferrimagnetic Fe oxide that has a Curie temperature of 850 K. As a mineral, it can be present in ilmenite with Ti contamination in the form of Titanomagnetite. This property is used in ilmenite separation from minerals such as rutile, leucoxene, zircon and monazite [30].
- $FeTiO_3$: Already introduced as ilmenite. Ilmenite's structure consists of a basic trigonal structure made of stacked oxygen layers separated by metal ion layers. Those metal ions alternate between layers of Ti^{4+} ions and Fe^{2+} ions. The Ti layers do not contribute to the magnetic moment, while the Fe layers are antiferromagnetic. However, the Neél

temperature of ilmenite is only of 60 K so it becomes paramagnetic at room temperature [31].

- FeO: Also known as wüstite, this Fe oxide is formed by oxidation of Fe and, if it is further oxidized it forms magnetite. It is antiferromagnetic until it reaches its Neél temperature of -70 °C. Then, it behaves as a paramagnetic material.

The oxidation states of iron go through the three Fe oxides previously introduced – wüstite, magnetite and hematite.

$$Fe \rightarrow FeO \rightarrow Fe_3O_4 \rightarrow Fe_2O_3 \tag{R11}$$

As it can be seen, the most oxidized phases reached are both magnetite and hematite. Magnetite is ferrimagnetic and hematite is antiferromagnetic at room temperature so ilmenite extracted from the boiler is expected to show magnetism, as it will have been present in an oxidizing environment. Even though there could be some lower oxidation forms formation like wüstite, it is not expected to be as abundant as magnetite and hematite in the combustion process and since it is paramagnetic it will not have much to do with the overall magnetic behaviour of the OC. Such behaviour is expected to be dictated mainly by hematite and magnetite [32].

The magnetic susceptibility data is scattered through the bibliography, so the chosen reference values for the magnetic susceptibility of these compounds will be consulted from John Dearing's Bartington MS2 Handbook (see [29]), the handbook for the magnetic susceptibility sensor that will be used in the experimental part of this report.

Table 1. Magnetic susceptibilities from Fe containing compounds. Extracted from "Table 2.2 - Minerals and magnetic susceptibility. Data from published and unpublished sources, showing ranges and individual measurements of susceptibility values and iron content" from [29].

Mineral/Material	Formula	Iron (mass%)	Mass specific magnetic susceptibility (10^6 m^3·kg^{-1})
Ferromagnetic			
Iron	Fe	100	276000
Ferrimagnetic			
Magnetite	Fe$_3$O$_4$	72	
(0.012-0.069 μm)			513-1116 500-1000
(0.09-2000 μm)			596±77
(1-250 μm)			440-716 390-580
Maghemite	β-Fe$_2$O$_3$	70	410.44
Titanomagnetite	Fe$_3$O$_4$-Fe$_2$TiO$_4$		169-290
Antiferromagnetic			
Hematite	α-Fe$_2$O$_3$	70	1.19-1.69 0.58-0.78 0.49-0.65 0.27, 0.31, 0.6, <0.63
Paramagnetic (20 °C)			
Ilmenite	FeTiO$_3$	37	1.7, 2

2 Methods

The main source of the data processed and shown in this report comes from characterization techniques such as Scanning Electron Microscopy, Energy dispersive X-ray spectroscopy, X-ray diffraction and X-ray fluorescence. Magnetic susceptibility measurements have also been conducted for some of the samples.

In this section, the working principle of each method is introduced, as well as the specific equipment used for each of them.

2.1 SEM-EDS

One of the main techniques for analysing the samples in this report is Scanning Electron Microscopy (SEM). SEM operation is based on the interactions between the surface atoms of the sample and a focused electron beam. Following this technique, the electron beam is accelerated with a high voltage from an electron gun that permits the electrons to penetrate further into the sample. As a result of this interaction between the surface atoms and the electrons of the beam, multiple signals are formed. These signals can be used for imaging (SE, BSE) and for characterizing (X-rays).

Each one of the signals provoked by the electron beam can be seen as originating from the interaction volume created by the beam in the analysed material. The interaction volume is the three-dimensional region of the sample where either elastic, inelastic or both interactions between the samples' electrons and the primary electron beam take place. This interaction volume is characterized as a teardrop shape where the different types of interactions appear in smaller specific volumes named escape volumes.
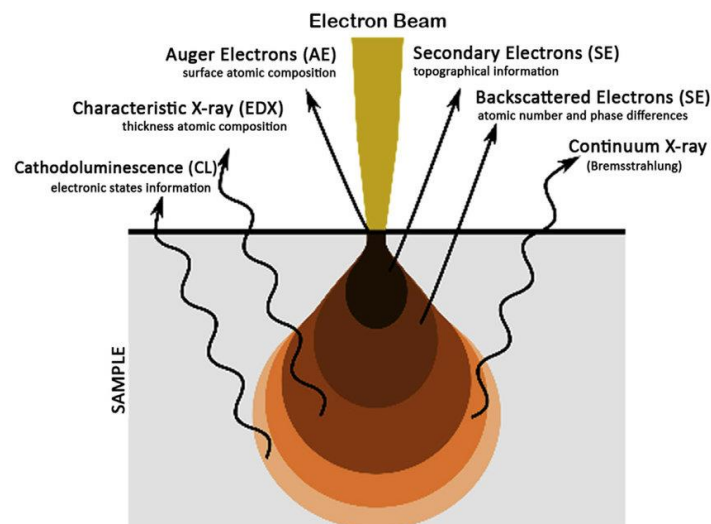
Figure 6. Illustration of the different signals that can be emitted from the interaction volume between the electron beam and the sample [33]**.**

The interaction volume can be of up to 5 μm and its size depends mainly on three different factors:

- Accelerating voltage of the beam. Higher voltages lead to a larger penetration from the beam in the sample. Consequently, a higher accelerating voltage also leads to an increase in the interaction volume.

- Angle of incidence of the electron beam or tilt. The more the angle of incidence of the beam towards the sample differs from the normal angle (90 degrees) the smaller the interaction volume is obtained.
- Atomic number of the sample's atoms (Z): Higher atomic number elements increase the elastic scattering (backscattering) and the interaction volume decreases. Another reason for that decrease is that when the atomic number is higher, the rate of energy loss is also higher and that contributes to a lower interaction volume [34].

Back-scattered electrons (BSE) are one of the signals which are used. These electrons are retro-dispersed or reflexed with elastic scattering when passing close to the core of the atom. The reflected electrons are then collected by a detector and a map image can be constructed through the analysis of every point and the number of back-scattered electrons.

BSE are used mainly to obtain information about the morphology of the sample and by the elemental contrast that points at the different chemical composition that there is in the sample. As BSE interact with the core, BSE SEM is a method that is dependent on the atomic number of the atom inspected. The brightness of the signal can help detect which areas of the sample are rich in heavier elements than others. When the signal is bright it means that more electrons are being backscattered and this means that the beam is being directed towards heavier atoms (in comparison to other areas of the overview).

Also, one of the most common signals used for SEM analysis is the presence of Secondary Electrons (SE). These electrons are produced by inelastic interactions between the electrons of the beam and the core electrons of the sample. In SE SEM the energy of the electrons of the beam is low (<50 eV) and thus only SE from the surface of the sample are yielded.

Another technique used in connection to SEM and used to characterize which elements are present in the sample is Energy dispersive X-ray spectroscopy (EDS). EDS basic working principle is that each element has a certain atomic structure that creates specific electromagnetic (X-ray) emission on the spectrum when an electron transfers from a higher energy level onto a lower energy level. When the high energy electrons from the beam interact with an electron from the shell it can excite the latter and provoke its release. The release leaves a hole that is filled by an electron from another energy level. While transferring to the lower energy level there is a release of energy in the form of X-ray radiation that can be measured. The energies of the X-ray released are specific for every element. An X-ray detector can convert the X-ray energy into Voltage that can be further processed.

EDS allows the identification of the different elements present on an analysed spot and their quantification in weight or atomic concentration. This way, it can accurately estimate the composition of the sample. With EDS one can analyse the chemical composition (concentration of elements) of the sample in points of interest, lines or in the form of intensity maps. The latter option maps the distribution of elements based on the difference in their concentration.

The equipment used for BSE-EDS in this report was a Phantom ProX Desktop SEM. For EDS, being an analytical method, it is recommended to select the mode operation meant for analysis: Analysis (15kV of Voltage). The detector mode selected was BSD Full and the intensity was selected as "map". For the pictures, the resolution was the highest (2048) and the quality of the acquired images was "High".

2.2 X-ray Diffraction (XRD)

The principle of X-ray diffraction (XRD) is based on the different crystal structures of the substances and how they diffract X-ray waves. Due to the different distribution of atoms in the cells of the crystal of minerals such as, for example, ilmenite, the incident X-ray wave can be diffracted into many different directions. The angles and intensity of the resulting radiation can be measured by a detector where the signal, in terms of intensity vs. angle of diffraction, forms a diffractogram from which information about the structure and distribution of the atoms in the crystal structure can be extracted.

The fundamentals behind the X-ray diffraction are that X-rays, which represent electromagnetic radiation with wavelengths in the nanometric scale, can interact with the electrons of the material. Interference occurs when the separation of the atoms of the sample is comparable in size to the wavelength of the X-rays.

The interference is considered constructive when the two X-ray diffracted waves are in phase with each other. When that happens, the amplitude of the wave that results adds up while the wavelength stays the same. Else, if the waves are not in phase, the interaction is considered destructive or partially destructive and the outcome is an X-ray wave that has a diminished amplitude compared to the other original two diffracted waves. In fact, if the interference is fully destructive the amplitude of the waves that result from the interaction is null.
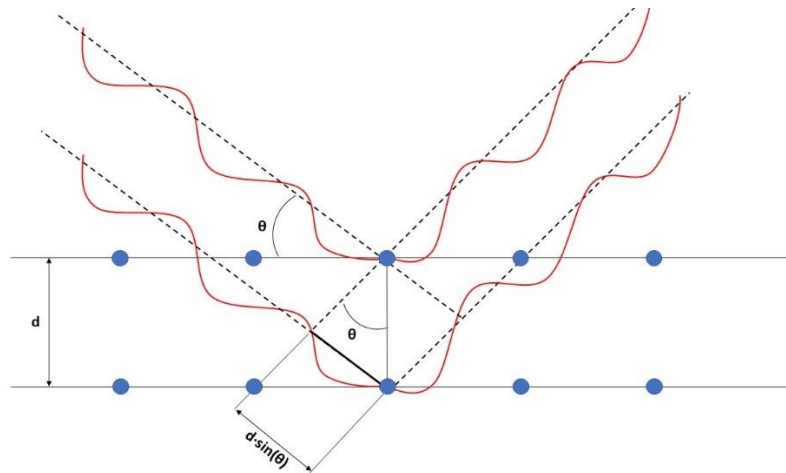
Figure 7. Illustration of the diffraction of X-rays in two planes of a crystallographic structure.

The type of interference is described by the Bragg's law. Bragg's law is as follows:

$$n \cdot \lambda = 2 \cdot d \cdot \sin (\theta)$$

where n is an integer (1, 2, 3 …) and it is the order of reflection of the scattered wave, λ is the wavelength of the incident X-ray beam, d is the distance between two consecutive planes of the molecular lattice and θ is the incident angle of the X-ray.

If the diffracted wave follows Bragg's law the interference is constructive. The classic instrumentation of XRD is an X-ray source (tends to be an X-ray tube) that emits focused X-ray beams towards the sample at a θ incident angle. That angle is increased with time so the detector receives a wide spectrum of scattered waves based on the angle of incidence of the source beam. The scattered waves can be analysed by a transducer that counts photons. The diffraction pattern can be compared to the diffraction pattern of reference materials available in a database. Based

on the coincidence of diffraction patterns, the crystalline compounds present in the sample can be identified [35].

The information obtained by XRD is the distribution and distances between the atoms inside the crystals and the length and type of their bonds, as well as the presence of any impurity in the sample. It gives information about the organization or packing of the atoms, which allows to match the identified structures to such that have a similar organization of atoms. Normally, these patterns are compared to those of a database and the structures are identified based on the comparison between the main peaks of the patterns and the index of adjustment to the data from the database.

XRD was performed in a Siemens D8 diffractometer. The samples were ground prior to the analysis and the patterns were compared to the database "Crystallography Open Database – REV212673" that the software DIFFRAC.EVA provides.

2.3 Magnetic susceptibility measurements

In this report, an analysis of the magnetic susceptibility of the sample was done by a Bartington MS2B magnetic susceptibility sensor. This sensor is connected to the MS3 Bartington device that connects to a computer in order to transfer the data to the Bartsoft computer program.

The relation between the permeability of air (the sensor approximates it to the permeability of the void) and the permeability of a specimen can give the value of the bulk magnetic susceptibility of a sample, according to the previously introduced Equation 3. The MS2B system measurement relies on the principle that any change in the permeability of a core causes a change of inductance in a wound inductor. Bartington sensors create a weak magnetic field from an alternating current (AC) and the frequency of oscillation is determined by the inductance of the system. At the same time, the inductance is dictated by the permeability of the system.

When there is no sample in the sensor, the magnetic permeability of air, which the sensor approximates to the vacuum permeability ($\mu 0$), determines the inductance, and at the same time the frequency of oscillation of the alternating current. When the sample is placed, there is a change in the oscillation of the alternating current that the sensor uses to calculate the change in inductance and therefore the difference in magnetic permeability. With that value, the magnetic susceptibility can be calculated according to Equation 3.

This device can measure susceptibilities of samples that are carefully placed in 12 ml. containers. The MS2B Sensor in particular, is a Dual Frequency Sensor, which means that it can measure the susceptibility at two different frequencies of the generated magnetic field. Thus, it has a Low Frequency (LF) mode (0.46 kHz) and a High Frequency (HF) mode (4.6 kHz). The results in HF mode are used for comparing with the LF results and if they do not match, it is an indicator of ultrafine ferrimagnetic particles with a diameter shorter than 0.03 μm. This is not expected in the samples analysed so the results have only been taken in LF mode.

Since there is a wide variety of magnetic susceptibility sensors and some sensors call for different methodologies, the methodology followed for the susceptibility measurements in the present report is further explained:

1. First, a drift test is conducted for 15 minutes with the magnetic susceptibility sensor. This warms up the sensors and prepares them for the measurements.
2. The calibration sample is measured to check whether the sensor is obtaining measurements that are exact enough. The measured value is compared to the nominal value provided by the manufacturer of the sensor.*

3. The 12 ml. empty container is weighted in an analytic balance and the measurement is written down.
4. The susceptibility of the empty container is measured before starting to measure a different sample.* The reason behind it is that some dust from other samples always accumulates inside and in order to make sure that it is not interfering or fouling the following measurements it has to be checked that its susceptibility is several orders of magnitude lower than that of the sample.
5. During the transport of the samples to Chalmers university from Örtofta, segregation between heavy and light elements/compounds might have occurred. It is possible that the heavy compounds tend to distribute near the bottom of the sample bottle whereas the lighter compounds may float to the top of the bottle. To prevent that, before extracting the sample from its bottle it is stirred so that a representative amount can be taken.
6. The container is filled up with the sample that is going to be measured. It must be filled up with sample completely until it can be scraped off the top of the pot with a spatula. Since the following weight measurement will be used for calculating the poured bulk density** it has to be done with caution and without tapping the container by accident.
7. The pot containing the sample is weighted again in an analytical balance. The mass of the sample that contains can be obtained by subtracting the weight of the empty pot to this last weight measurement.
8. An Individual Test is selected in the Bartsoft software.
9. The options selected for the measurement are a 5 second Blank test followed by a 10 second sample measurement and another 5 second Blank test. For the Blank test no sample should be placed in the susceptibility sensor and only after the first Blank measurement the sample should be placed inside the MS2B sensor.
10. Steps 5 and 6 are repeated three times in order to have more than one value and see the deviation of the measurements.

* The steps that are marked with this symbol follow the same susceptibility measurements that follow steps 8 and 9.

** The poured bulk density refers to the density of the sample that is obtained by introducing the sample inside of the container without moving or tapping it. If it is tapped, the free space present between the particles will be filled with other particles and then the volume decreases. This method was chosen due to its quickness, reproducibility and scarce requirements of equipment that makes it suitable for the industrial stage of measurements.

The value obtained with the sensor is the volumetric magnetic susceptibility of the bulk of the sample. However, not every sample has the same mass and not every measurement present in the bibliography is measured in 12 ml containers. Since the volumetric magnetic susceptibility value depends on the mass and volume of the sample measured, it has to be divided by the bulk density of the sample in order to be comparable with other sample measurements and with data from the bibliography. In the present report, the value of the density corresponds to the poured bulk density. If calculated following Equation 4, the mass specific magnetic susceptibility is obtained:

$$\chi_{mass} = \frac{\chi}{\rho} \ (\frac{m^3}{kg}) \tag{E4}$$

Where χ_{mass} is the mass specific magnetic susceptibility, χ the magnetic susceptibility and ρ is the bulk density of the sample that is measured. For convenience, from this point on, in the report the

"mass specific magnetic susceptibility" will be referred as "magnetic susceptibility" as it is the value that will be compared.

2.4 X-ray Fluorescence (XRF)

X-ray fluorescence (XRF) is a non-destructive analytical technique used for the quantification of the bulk elemental composition of materials.

The principle behind it stems from the use of primary high-energy X-rays or gamma rays to excite the core-level electrons from the sample towards an excited state. The hole left by that excited electron will be eventually filled by an electron from a higher energy state that decays and that results in the emission of a characteristic secondary X-ray. These emitted secondary X-rays (also known as fluorescent X-rays) have a lower energy than the incident primary ones. The energy of the secondary X-rays is characteristic of every element as it gives information about the energy levels of the atomic species and their differences in energy [36].
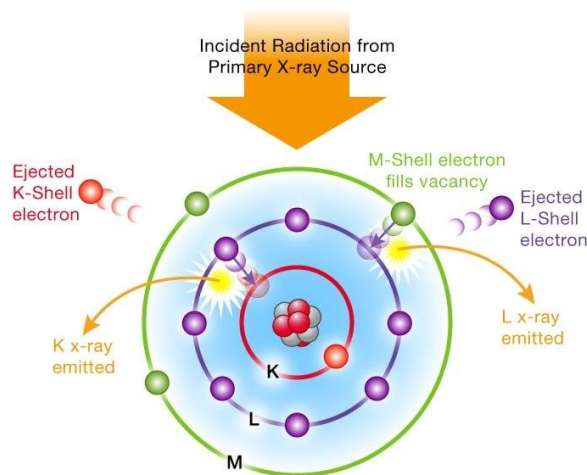
Figure 8. Illustration of the incident X-ray radiation hitting the atom and the resultant X-ray fluorescence emission [37]**.**

An X-ray detector can convert the X-ray energy into a voltage that can be processed and then a spectrogram can be obtained from it.

The method allows for quantification of the elemental composition in the sample since the intensity of the secondary X-rays is proportional to the abundance of the elements in the material [38].

The fundamentals behind the technique are similar to SEM-EDS, but the incident radiation directed towards the sample in each technique is different. SEM-EDS uses a focused electron beam while XRF uses short wavelength X-rays. In some cases, both techniques even use the same detector. However, generally, XRF is able to give deeper information since it typically detects elements at the ppm level, while EDS usually has a detection limit at the 0.1% level (it can vary depending on the electron beam acceleration voltages applied) [39].

XRF allows the identification of the different elements present in the bulk phase of a sample and their quantification in atomic concentration. This way, it can accurately estimate the composition of the sample. With XRF it is possible to analyse the chemical composition of the bulk phase, not only specific spots, lines or intensity maps as it happens with EDS.

XRF was performed with a PANalytical Axios spectrometer and it was made sure that the samples covered the whole bottom of the support so that no holes were present when the analysis took place. To do so, a weight of approximately 4-5 g was introduced in the sample holder.

3 Results

In this section, the results of the analytic methods and the magnetic susceptibility measurements are presented. The outcomes of each method are presented here as well as some observations while the connections between the results can be found in the Discussion section.

The first thing that was done was creating a code to name all the samples that were initially considered in an easy way. More information about the code and its meaning can be found in Appendix I.

SEM-EDS results will be presented in the first place, followed by XRD, magnetic susceptibility measurements and XRF respectively.

It was decided to investigate about the differences in the magnetically separated fractions of an industrial sample (Örtofta samples) and how that can be related to a function of available free Fe and interactions with the ash compounds. The main questions of interest that follow that analysis are how this magnetic separation is handled in an industrial size boiler and if the process of recirculation of ilmenite can be improved.

That is why the efforts were focused on the bottom ash samples from Kraftringen's CFB boiler located in Örtofta (Skåne, Sweden) that appear in the Appendix I.

The analysed samples are from a three-week campaign that was run in Kraftringen's CFB boiler from the 4th of April to the 22nd of April of the year 2018. The CFB boiler has a nominal thermal capacity of 115 MWth and it is normally operated with quartz sand but in that campaign, the bed material was replaced for oxygen-carrying rock ilmenite that comes from the Tellnes mine owned by Titania (in Norway). The fuel used was a mix of waste wood and wood chips.

When analysing samples that come from an industrial boiler several things have to be taken into account. The fuel that is fed at the Örtofta plant is very heterogeneous. That means that it should be expected to find a quite large number of different elements in the SEM-EDS and XRF analysis.

In industrial facilities the composition of the fuel is varying also from one time point to another and between the plants. Also, when a change of fuel or operational conditions is done, a change in the actual bed tends to happen with a delay of one or a few days (this delay is not homogeneous in time). That same phenomenon happens if one models the boiler as a CSTR, where a change in the feed provokes a change in the internal conditions of the reactor. That change can be extended in time and one of the variables that dictates how fast/slow it appears is the amount of inlet material compared to the material present in the actual reactor. In the case of the Örtofta boiler, the amount of matter it contains is quite big as it has a capacity of 60 tons of bed material under normal operation.

The location in the combustor from where the samples of bottom ash are extracted can vary from one combustion unit to another. That means that the bottom ash may be extracted from varying locations in boilers of different CHP plants. In the case of the Örtofta plant, it is extracted from the bottom of the boiler. The plant conditions differ from one facility to another and therefore

conclusions should be made predominantly for the studied case at Örtofta and data should be carefully used to draw more general conclusions.

All of these considerations imply that the results obtained should be initially related to the Örtofta plant and specifically to the campaign that was held for the month of April (from the 4th of April to the 22nd of April) of 2018. That does not necessarily mean that a general trend or a representative phenomenon cannot be observed or pushed forward in other power plants but rather that the limitation should be taken into consideration.

It would have been interesting to evaluate the fly ashes from the Örtofta combustor to check if there is attrition of Fe going on and if so, when does it start. However, there were no available fly ash samples from Örtofta. At this point, it was decided to use the available resources and a simplification was proposed. Since the available fly ash samples were from a campaign run on the Chalmers 12 MWth CFB boiler during the winter of 2014, it was assumed that the semi-industrial-size boiler can be similar to the fully industrial-size facility located at Örtofta. The fuel used in that campaign was wood chips and their composition can be checked in Corcoran et al [21]. The findings under this assumption will need to be revisited in future work as the assumption will not be proven true in this project. This assumption is done, thus, for explanatory purposes.

3.1 SEM-EDS results

SEM-EDS was used both for imaging and chemical analyses. For imaging, several micrographs of the surface of the sample were taken. They were used to follow the morphology development for the different samples. For chemical analysis, EDS point analysis were performed on selected locations. All of the analysis results are normalized on a C and O free basis. This normalisation is required because C and O are common elements and thus their quantification is not possible. The results have to be analysed, then, without taking them into account.

First, a preliminary point analysis was performed on selected particles from the Örtofta samples to see if there was something that stood out from the samples.

When observing the samples from Örtofta separated by the magnetic separator, the following observations were made: 1) Morphology of the particles, 2) similarities and differences in chemical composition and 3) artifacts, particles that are not expected in each fraction, such as feldspar in the magnetic fraction and ilmenite in the magnetic reject.

After that, the share of artifacts and ilmenite particles in each sample was quantified thanks to point analysis with EDS. The surfaces of selected artifacts and an ilmenite particle from the magnetic fraction Ört-0417-MF were also analysed with point analysis in EDS.

Lastly, SEM-EDS was also used for attempting to see if attrition of Fe happened in the Chalmers boiler campaign in 2014. The samples analysed for this purpose are the particles from the cyclone of the same boiler.
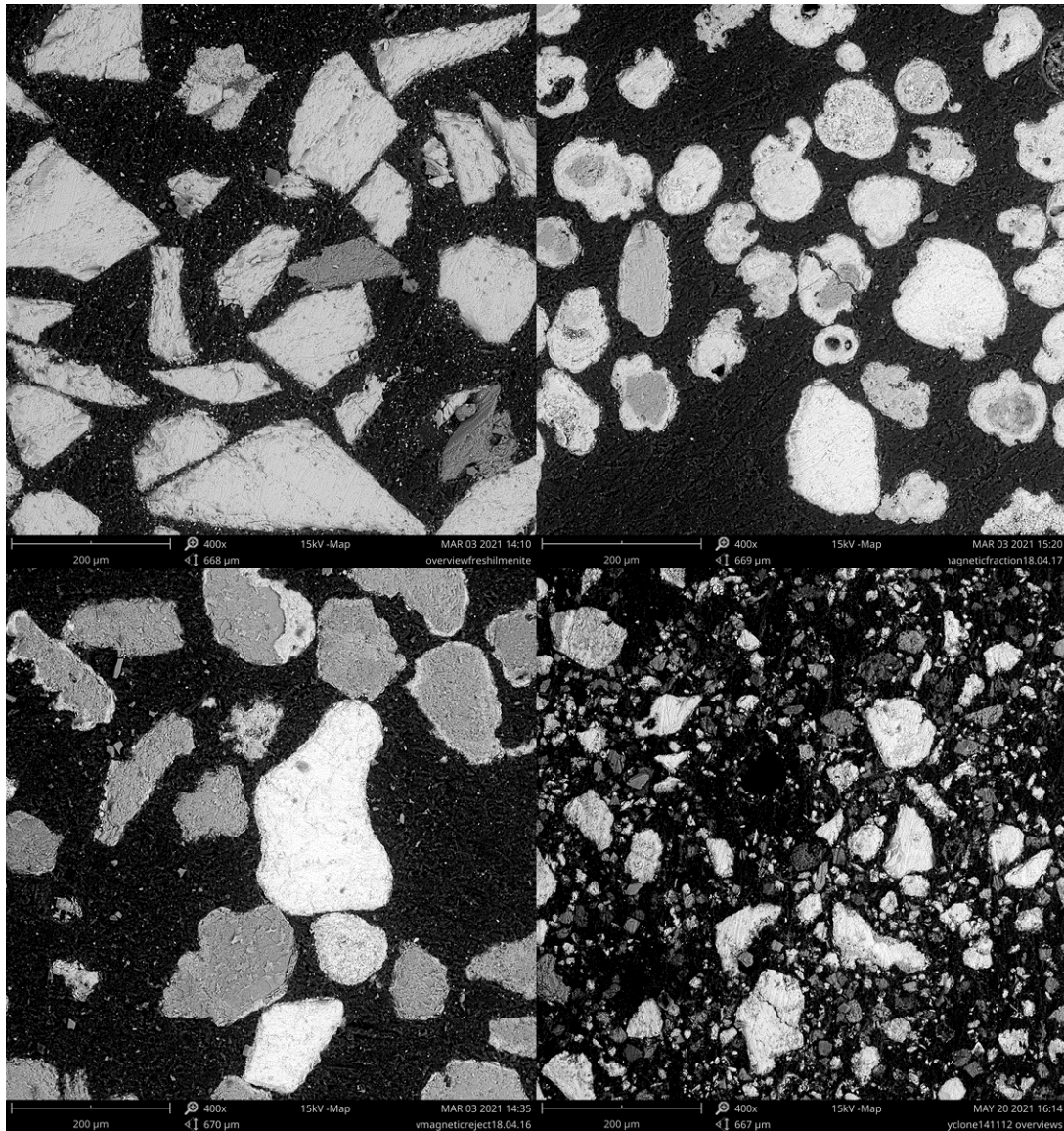
Figure 9. BS SEM micrographs of the samples: Fresh ilmenite (Top left), Ört-0417-MF (Top right), Ört-0416-RF (Bottom left) and Cyk-1125-OCAC (Bottom right).

After performing preliminary point analysis on selected particles of the Örtofta samples and comparing them to the Fresh ilmenite sample as well as the fly ash samples from the cyclone, several findings were noted:

1. The fresh ilmenite particles already contain Mg (mainly in the form of single feldspar particles or ilmenite particles attached to feldspar particles) and that seems to be the main source of Mg for the samples extracted from the boiler. The Örtofta samples also have these feldspar particles, even in the magnetic fraction. This last finding especially stands out as feldspar is not magnetic.
2. There are ilmenite particles in the magnetic reject fraction. That also stands out as ilmenite, after undergoing oxidation, tends to have formed Fe oxides that show magnetic properties, oxides such as magnetite or hematite.
3. After more operation time, the concentrations of Ca and K have effectively risen. That is, the point analysis shows that the particles from April 17 have higher concentrations of these two elements than the samples from April 9.

26

4. As it can be seen in Figure 9, particles in the cyclone sample are smaller compared to bottom ash (as it should be for fly ash) and contain a lower concentration of K.

In order to answer the question regarding the presence of feldspar particles in the magnetic fraction, two things were considered. First, it has to be quantified the share of these feldspar particles in the fresh ilmenite and the Örtofta samples to make sure about the origin of the particles and whether it happens consistently in the samples. It also needs to be made sure whether what was observed with SEM-EDS is representative for the samples. Second, an initial hypothesis was raised. The hypothesis was that the feldspar particles that appear in the magnetic fraction are covered in some type of Fe rich layer that has magnetic properties and that is why they end up being dragged onto the magnetic fraction container when they are separated from the blend.

Similar considerations were taken when approaching the presence of ilmenite in the magnetic reject. The initial hypothesis, in this case, is that the particle has either lost the magnetic Fe oxides that may migrate to the surface due to attrition, that the particle has not been oxidized enough or that the ash layer somehow is so thick that it strongly affects the magnetic susceptibility of the particle.

To quantify the ilmenite and feldspar share of these particles, 6 overviews were taken with SEM of the following samples immobilized in epoxy: Fresh, Ört-0409-BA, Ört-0416-RF, Ört-0417-MF, Ört-0417-BA. The overviews are SEM micrographs taken with the lowest magnification possible (400X) in the tabletop SEM that was used during the experimental part. These micrographs were used to identify the share of the type of particles in each studied representative sample. In order to not introduce bias when choosing the locations of the overviews, they were always taken in the same 6 positions. A further explanation of how that was done can be found in the Appendix II.

To appreciate the distribution of the particles in each sample, point analysis with SEM-EDS was performed on the particles with a diameter bigger than 100 μm in the overviews of each sample. Based on the element concentrations of the particles, they were classified as ilmenite, feldspar, ilmenite-like particles and other particles, and a share of each type of particle was calculated for each overview. That classification would allow to see the deviations in the bulk composition of the samples and their shares of each of the particles of interest (ilmenite and feldspar mainly).

After OCAC operation, ilmenite particles that have reacted with the fuel ashes can have a quite diverse composition. That complicates the classification of the particles. The way it has been done is that if the particle shows a considerable atomic % of both Fe and Ti, but also ash elements like Ca, K or Si, the particle can be considered as an ilmenite-like particle or derived from it. If the particle has a predominantly high concentration of Fe and Ti compared to the elements present in ash compounds, then it is classified as an ilmenite particle. If a particle is not classified as neither ilmenite-like, ilmenite or feldspar particle, then it is taken into account as "other particles".

The following Table 2 shows the number of ilmenite, ilmenite-like and feldspar particles in each one of the 6 overviews taken from the samples and the sum of the number of particles of all overviews for each sample and the corresponding shares. It can be seen that the sum of ilmenite, feldspar and ilmenite-like particles does not equal the total number of particles that were accounted for. That is because there were particles that could not be classified as neither of the three but they were accounted for the total number of particles due to having a diameter larger than 100 μm.

Table 2. Shares of ilmenite, feldspar and ilmenite-like particles in the overviews of the Fresh ilmenite sample and four Örtofta samples.

Overview	Fresh*							Ört-0416-RF**						
	1	2	3	4	5	6	SUM	1	2	3	4	5	6	SUM
Number of ilmenite particles	14	19	18	11	20	18	100	2	2	1	2	2	3	12
Number of feldspar particles	0	0	0	0	0	2	2	10	16	15	14	7	13	75
Number of mixed particles* Number of ilmenite-like particles**	1	1	0	2	1	0	5	0	0	0	0	0	0	0
Number of particles	15	20	18	13	21	21	108	12	18	16	16	9	16	87
% of ilmenite	93	95	100	85	95	86	**93**	17	11	6	13	22	19	**14**
% of feldspar	0	0	0	0	0	10	**2**	83	89	94	88	78	81	**86**
% of mixed particles	7	5	0	15	5	0	**5**	0	0	0	0	0	0	**0**
% of ilmenite or mixed particles* /ilmenite-like particles**	100	100	100	100	100	86	**97**	17	11	6	13	22	19	**14**

Overview	Ört-0417-MF							Ört-0409-BA						
	1	2	3	4	5	6	SUM	1	2	3	4	5	6	SUM
Number of ilmenite particles	1	0	0	0	0	0	1	2	1	3	1	0	2	9
Number of feldspar particles	3	3	3	0	3	2	14	3	6	3	4	6	5	27
Number of ilmenite-like particles	7	11	11	13	8	9	59	4	8	6	7	8	6	39
Number of particles	12	16	16	17	12	12	85	16	18	15	17	17	14	97
% of ilmenite	8	0	0	0	0	0	**1**	13	6	20	6	0	14	**9**
% of feldspar	25	19	19	0	25	17	**16**	19	33	20	24	35	36	**28**
% of ilmenite-like particles	58	69	69	76	67	75	**69**	25	44	40	41	47	43	**40**
% of ilmenite or ilmenite like particles	67	69	69	76	67	75	**71**	38	50	60	47	47	57	**49**

Overview	Ört-0417-BA						
	1	2	3	4	5	6	SUM
Number of ilmenite particles	0	0	0	0	0	0	0
Number of feldspar particles	2	2	0	4	3	0	10
Number of ilmenite-like particles	8	9	14	8	14	16	69
Number of particles	11	12	16	15	18	17	89
% of ilmenite	0	0	0	0	0	0	**0**
% of feldspar	18	17	0	27	17	0	**12**
% of ilmenite like particles	73	75	88	53	78	94	**78**
% of ilmenite or ilmenite like particles	73	75	88	53	78	94	**78**

Out of the shares the following information can be extracted:

- The blend Ört-0409-BA sample has a substantial share of particles that are not ilmenite neither feldspar (i.e. particles where the only two main elements are Si and Ca) so the share of ilmenite, feldspar or ilmenite-like particles is lower consequently.

- The share of ilmenite (only accounts for the ilmenite particles that have a similar composition to that of the fresh ilmenite, i.e. without having major ash compounds in their structure) found in the magnetic reject is bigger than the one found in the magnetic fraction (Ört-0417-MF) and blend (Ört-0417-BA). However, that does not take into account the number of ilmenite-like particles or particles derived from ilmenite, which added up to the % of ilmenite stands for a bigger share in the magnetic separation blend (both from day 9 and day 17) and fraction samples. That seems to indicate that the particles that react more with the ash compounds end up in the magnetic fraction rather than in the reject.
- The feldspar share of the magnetic fraction Ört-0417-MF (17%) is quite high for being the magnetic accept as feldspar should fall with the non-magnetic fraction. This number is also higher than the feldspar share of the Ört-180417-BA (12%) which is the blend before magnetic separation. If the magnetic separation is being handled correctly, the bulk magnetic fraction should have a lower % of feldspar than the bulk blend before separation. This phenomenon can be explained mainly because of the heterogeneity of the Örtofta samples. Given that heterogeneous mixture, obtaining a representative fraction from the bottom ash as a whole and then taking a representative overview may result in this type of deviations. The % difference between both samples is only 5%, which considering the order of magnitude of the particles accounted for (85 and 89 for Ört-0417-MF and Ört-180417-BA respectively) is a low discrepancy or at least it is not aberrant.

In order to correlate the share information to the hypotheses that were previously suggested, an analysis of the layers of the ilmenite particles of the magnetic reject and the fresh ilmenite was performed. To represent the variation of the atomic % close to the edge of the particles, several points of each particle were analysed with EDS and represented in the following Figures 10 to 12. The successive point analysis performed in the same particle were done in a way that they followed a straight line. Also, the first point analysis was done starting from the point farthest to the surface and each point analysis that followed was performed closer to the surface of the particle. That is why it should be noted that in these Figures where atomic % is represented against the location of the particle, the X axis is increasingly close to the edge of the particle (i.e. the highest number in the axis represents the edge of the particle).

The Fe:Ti ratio is also represented to see if there is any difference in Fe distribution along the particle.

As an example of how the points were taken in the sample, the next Figure 10 (left) also illustrates the analysis of the surface of an ilmenite particle from the fresh ilmenite sample.

First, the surface of an ilmenite particle from the fresh ilmenite is compared to one from an ilmenite particle from the magnetic reject (Ört-0416-RF), so that it is possible to observe differences that may have to do with the loss of magnetism. The distribution of Fe, Ti and Si elemental concentrations as well as the Fe:Ti ratio from Fresh ilmenite along the line of points is also represented in Figure 10 (right). The same representation is done in Figures 12 and 31 but for ash elements Al, Ca, Na and K. This is done so that it can be seen how Fe, Ti and ash elements distribute along the particle, which may indicate if an ash layer is detected in the reject particles and if a case for Fe migration can be done. In case a layer is detected, it will be detected by comparing with the fresh ilmenite distribution, that does not present a layer.
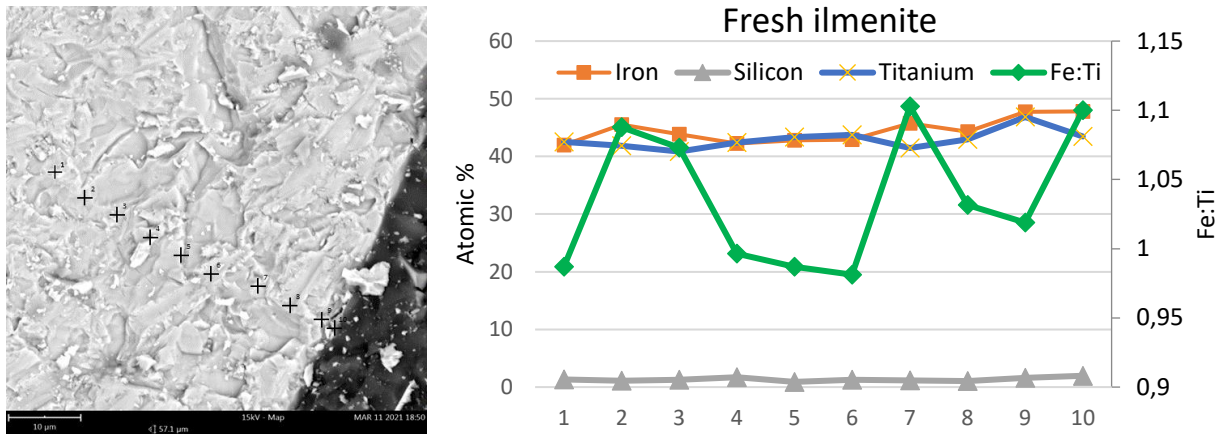
Figure 10. Left: BS SEM micrograph of the chosen points for the performed SEM-EDS scan, fresh ilmenite. Right: Elemental distribution for Fresh ilmenite particle. The distribution of Si, Fe, Ti and Fe:Ti is plotted from a location near the core of the particle (1 in the X-axis) to the surface of the particle (10 in the X-axis).

As it was previously introduced, the same analysis was performed on the magnetic reject (Ört-0416-RF) sample.

Figure 11. Elemental distribution for Ört-0416-RF ilmenite particle. The distribution of Si, Fe, Ti and Fe.Ti is plotted from a location near the core of the particle (1) to the surface of the particle (6).

Then, the distribution of several ash compounds (Al, Ca, Na and K) obtained with EDS in the same way as before is presented in Figures 12 and 31 in order to determine if there has been ash layer formation.

No ash compounds can be found in the fresh ilmenite particle so there is no distribution that can be represented. The graphic distribution is located in the Appendix III (Figure 32).

Figure 12. Elemental distribution for Ört-0416-RF ilmenite particle. The distribution of Al, Ca, Na and K is plotted from a location near the core of the particle (1) to the surface of the particle (6).

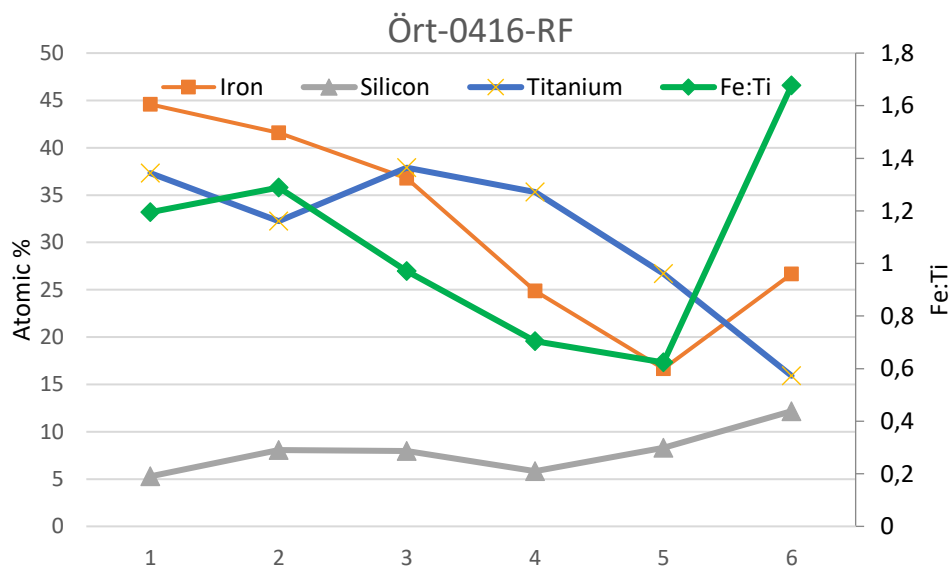As it can be seen, the surface of the ilmenite particle from Ört-0416-RF shows a higher concentration of ash elements than its core, where the concentration is closer to zero. The BS SEM micrograph of that particle and its surface is presented in Figure 13 to see if a layer can be observed.
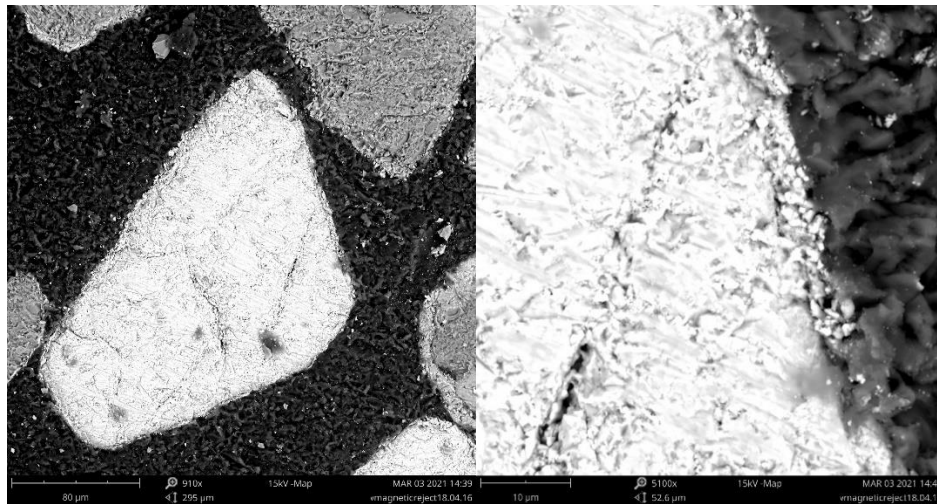
Figure 13. SEM micrograph of ilmenite particle from the magnetic reject fraction (Ört-0416-RF) with the surface analysed in Figure 11 and 12.

- From a visual and morphological standpoint, it can be seen that the surface of the reject particle presented in Figure 13 has a much more heterogeneous surface than the surface of the fresh ilmenite presented in Figure 10.

- Comparing the ilmenite particle from the fresh ilmenite and the ilmenite particle from the magnetic reject Ört-0416-RF it can be seen that both Fe and Ti decrease in concentration when approaching the surface of the particle in the magnetic reject fraction whereas in the fresh ilmenite the share stays considerably constant. This can be explained by the fact

that since there is a higher concentration of ash close to the surface, both Ti and Fe concentrations decrease. However, the Fe concentration decreases less in comparison with Ti concentration (and therefore, the Fe:Ti ratio rises) for the last point that is closest to the surface (6). This could mean that there is some Fe migration towards the surface, even though an ash layer seems to be prevalent. The relative increase between the Fe:Ti ratio of the point closest to the particle core (point 1) and its maximum Fe:Ti, which would be the place where an Fe layer is present, is of about 40.3% for the reject while for the fresh ilmenite particle it is of about 11.7%.

A case could be made for Fe migration in the ilmenite particle from the reject but in any case, an ash layer that appears to be not magnetic (as the particle is in the magnetic reject) is formed outside of the particle when operating.

- There are no ash components in the fresh particles. However, some particles with a feldspar part attached to them can be seen (See the top left micrograph in Figure 10 for an example). This comes from the way ilmenite particles are mined and purified in the Tellnes mine owned by Titania in Norway [25, 26].

Regarding the presence of feldspar particles in the magnetic fraction, the same layer analysis was performed of one feldspar particle of the magnetic accept and one feldspar particle of the magnetic reject. For the feldspar particle from the magnetic fraction Ört-0417-MF, the distribution of Fe, Ti and Si is presented in Figure 14, the distribution of ash elements is presented in Figure 15 and the micrograph of the particle analysed as well as its layer are both presented in Figure 16. For the feldspar particle from the magnetic reject Ört-0416-RF, the respective Figures are Figure 17, Figure 18 and Figure 19.

Figure 14. Elemental distribution for Ört-0417-MF feldspar particle. The distribution of Si, Fe and Ti is plotted from a location near the core of the particle (1) to the surface of the particle (8).
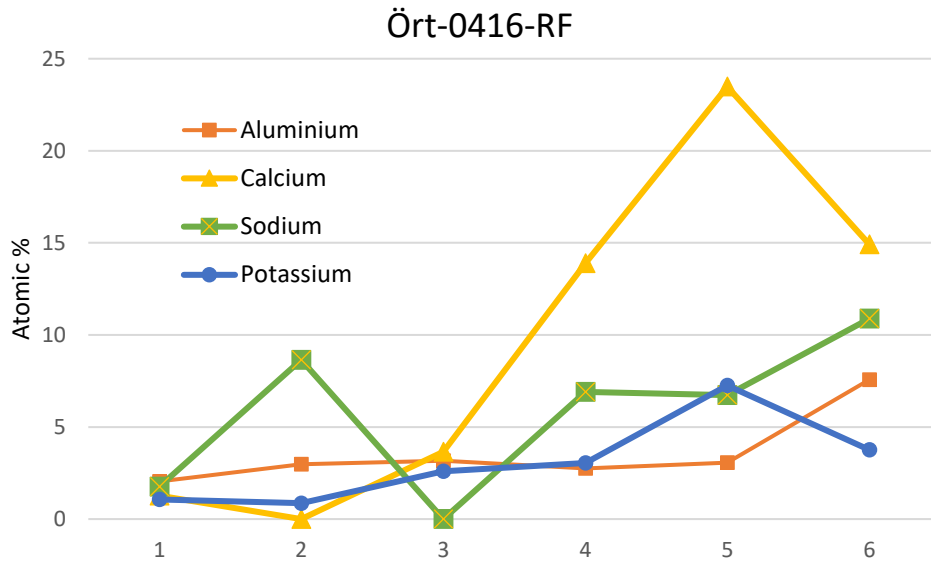
Figure 15. Elemental distribution for Ört-0417-MF feldspar particle. The distribution of Al, Ca, Na and K is plotted from a location near the core of the particle (1) to the surface of the particle (8).

Figure 16. BS-SEM micrograph of a feldspar particle from the magnetic fraction (Ört-0417-MF) and surface analysed in Figure 14 and 15.

33

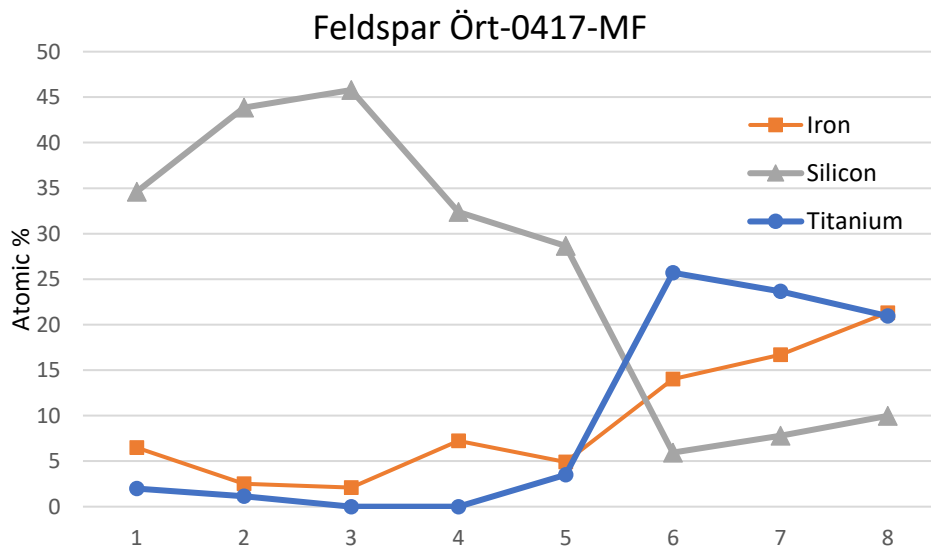**Figure 17. Elemental distribution for Ört-0416-RF feldspar particle. The distribution of Si, Fe and Ti is plotted from a location near the core of the particle (1) to the surface of the particle (5).**
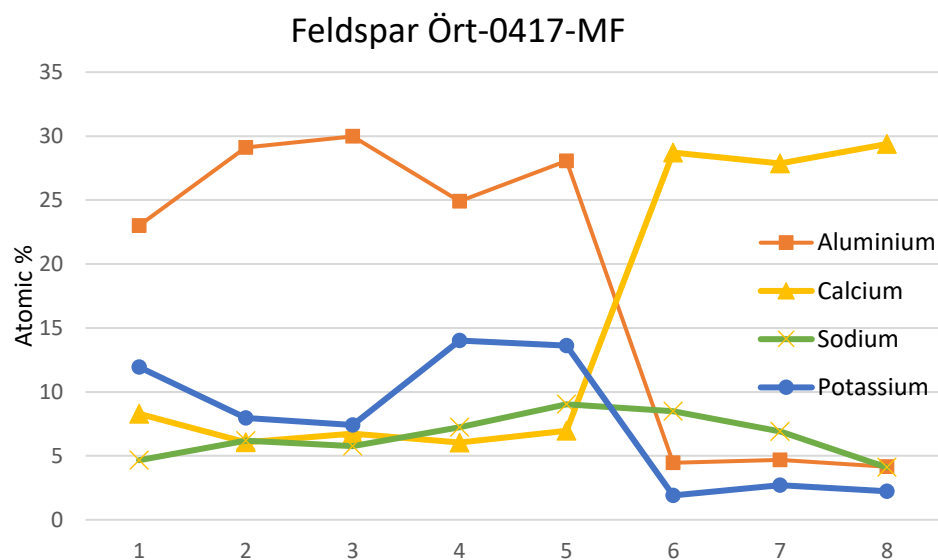

Figure 18. Elemental distribution for Ört-0416-RF feldspar particle. The distribution of Al, Ca, Na and K is plotted from a location near the core of the particle (1) to the surface of the particle (5).
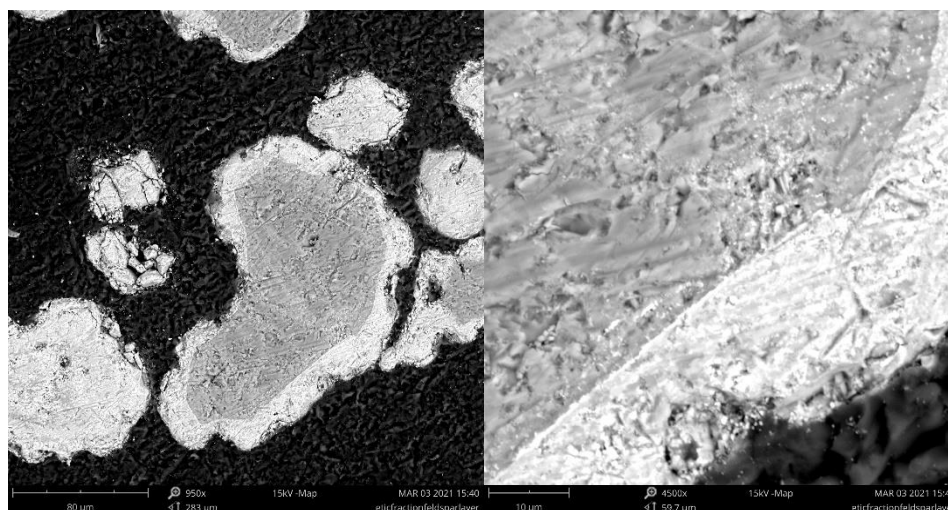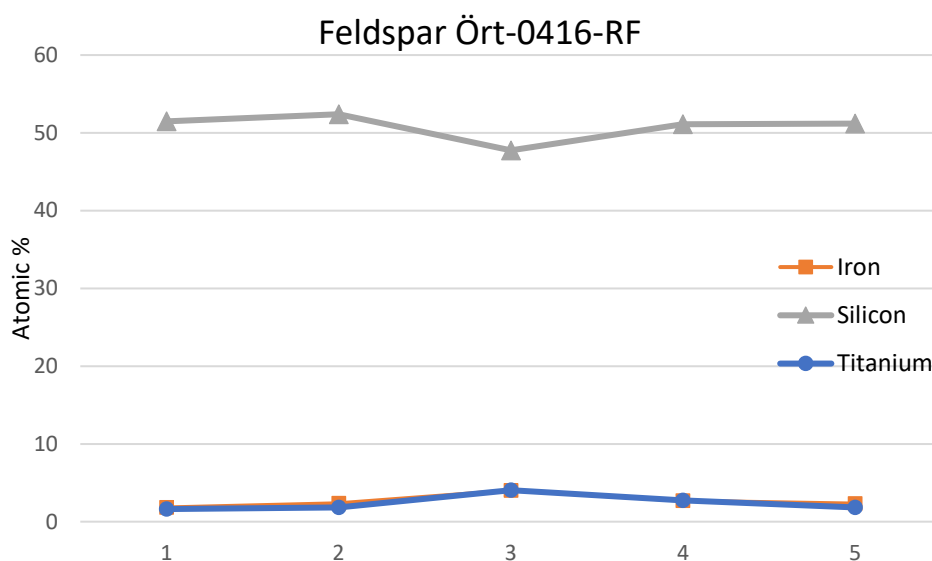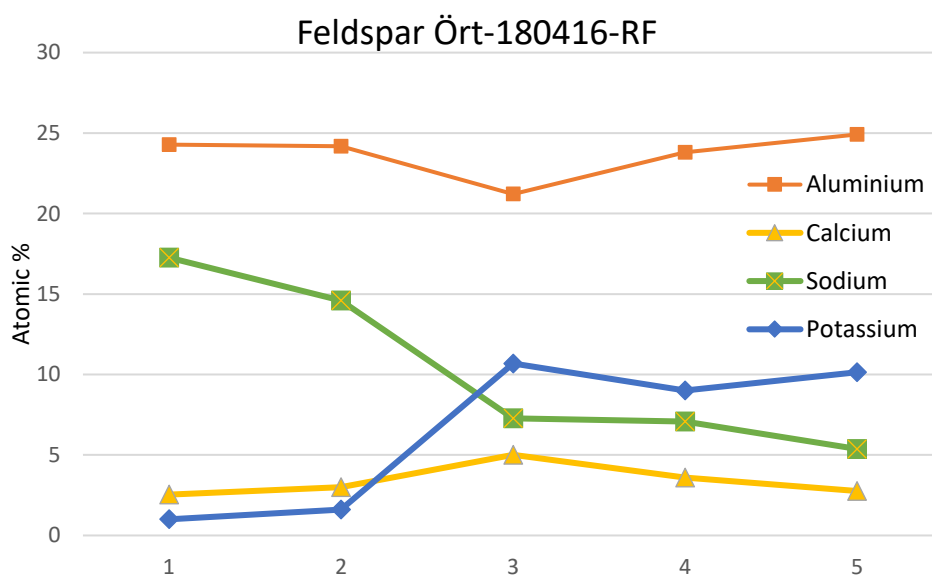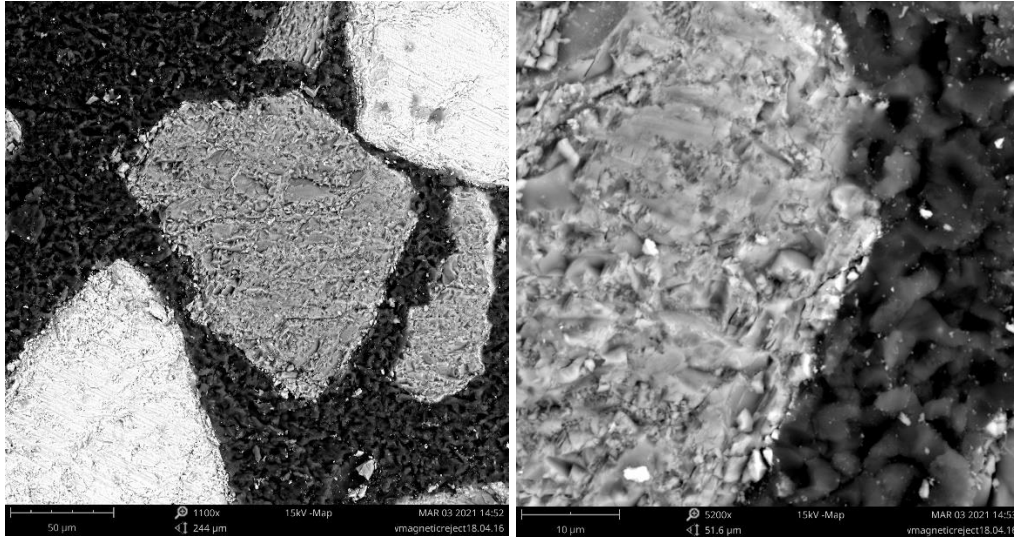
Figure 19. BS-SEM micrograph of a feldspar particle from the magnetic reject (Ört-0416-RF) and surface analysed in Figure 17 and 18.

Three main observations can be made regarding the feldspar particles of Ört-0416-RF and Ört-0417-MF.

- From a visual standpoint, the feldspar particle from Ört-0417-MF in Figure 16 seems to show a layer that can be seen in a lighter colour than the Ört-0416-RF feldspar particle appearing in Figure 19. This means that it is made of elements with a higher atomic number. Considering the K-feldspar structure that consists of Al, Si and K, these heavier elements present in the lighter surrounding area could be Ca, Ti, Fe or all of them. Looking at their respective concentration distributions in Figure 14 and 15, it can be seen that all of them seem to be in that layer.

- It can be stated that feldspar particles in the magnetic fraction have a layer with a high composition in Ca, Fe and Ti. This has been observed on selected feldspar particles and it could explain why there is feldspar in the separated fraction that should be magnetic. The Fe compound should be magnetite, hematite or another compound with a high enough magnetic susceptibility if it goes with the magnetic accept.

- The feldspar particles of the magnetic reject have a much more stable composition across the particle than the feldspar particles collected in the magnetic fraction. The composition of the feldspar particles from the magnetic reject does not seem to vary substantially along the particle (except for K and Na).

After the analysis of these artifacts present in the magnetic fraction and the magnetic reject, SEM-EDS was also used for analysing if the particles from the magnetic fraction had developed an Fe layer. The same point analysis process was followed for this analysis. However, in this case, the relevant information comes from the concentration of Fe oxides that could be present close to the surface of the particle. According to the bibliography, the surface of the particle is expected to have ash compounds attached in the form of an ash layer. That is why measuring and representing the elemental concentration of Fe can be misleading as the composition close to the surface of the particle is more heterogeneous and as a result, the Fe concentration may appear to be lower. Instead, what will be looked at in order to determine if there has been a migration of Fe is the Fe:Ti ratio. The concentration of Ca in atomic % will also be presented to see if it also presents an accumulation of Ca close to the surface.

The particle analysis was performed in two different ilmenite particles from the magnetic fraction Ört-0417-MF. Figures 20 and 22 show a BS-SEM micrograph of the particle and its surface for particle 1# and 2# respectively, while Figures 21 and 23 show their respective Fe:Ti ratio and the Ca concentration distribution along the surface of the particle.
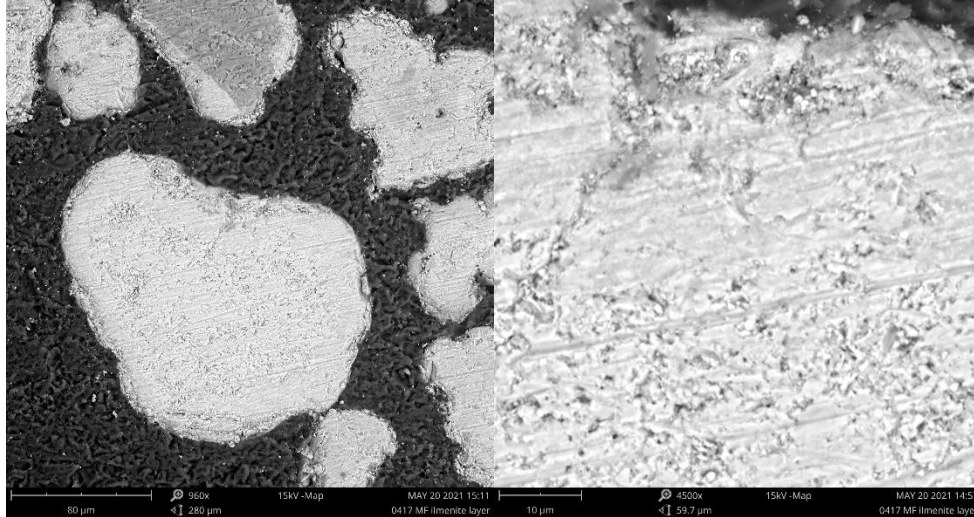
Figure 20. BS-SEM micrograph of ilmenite particle #1 (left) from the magnetic fraction (Ört-0417-MF) and surface analysed (right) in Figure 21.

Figure 20 (right) shows the surface of the particle, which appears to be more heterogeneous than the core of the particle.
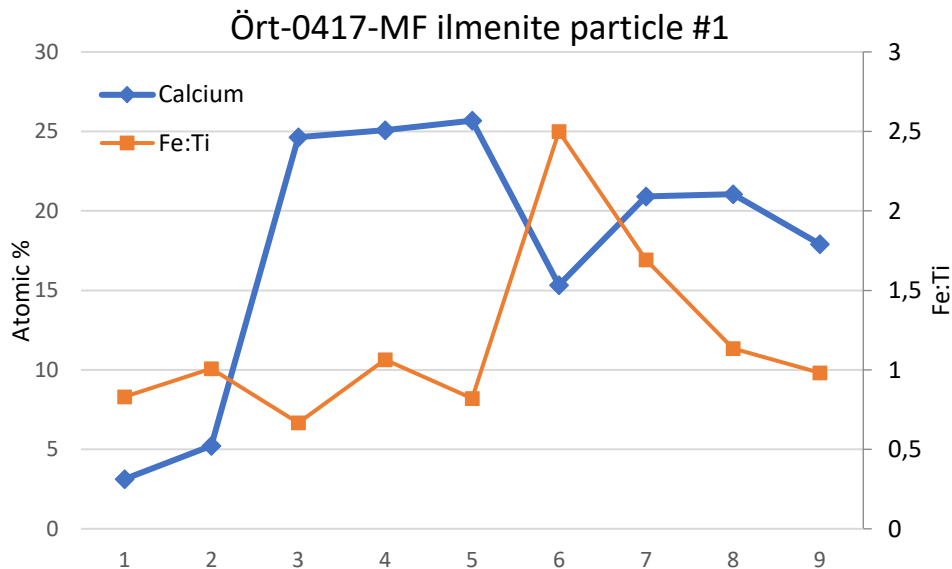
Figure 21. Fe:Ti ratio and elemental concentration of Ca in ilmenite particle #1 from Ört-0417-MF. The ratio and the concentration are plotted from a location near the core of the particle (1) to the surface of the particle (9).

Figure 21 appears to show that where Ca concentration is high, the ratio between Fe and Ti decreases and vice versa. There is an increase in Fe concentration around the points 6 and 7 that could be indicating the presence of an Fe layer. The Fe:Ti ratio relative increase between point 1 (the closest to the particle core) and the maximum Fe:Ti ratio is 201%. Also, the increase in Ca

36

for the closest points to the surface of the particle (points 7, 8 and 9) could be signalling the formation of a Ca double layer that was observed in earlier bibliography. This will be further discussed in the Discussion section.
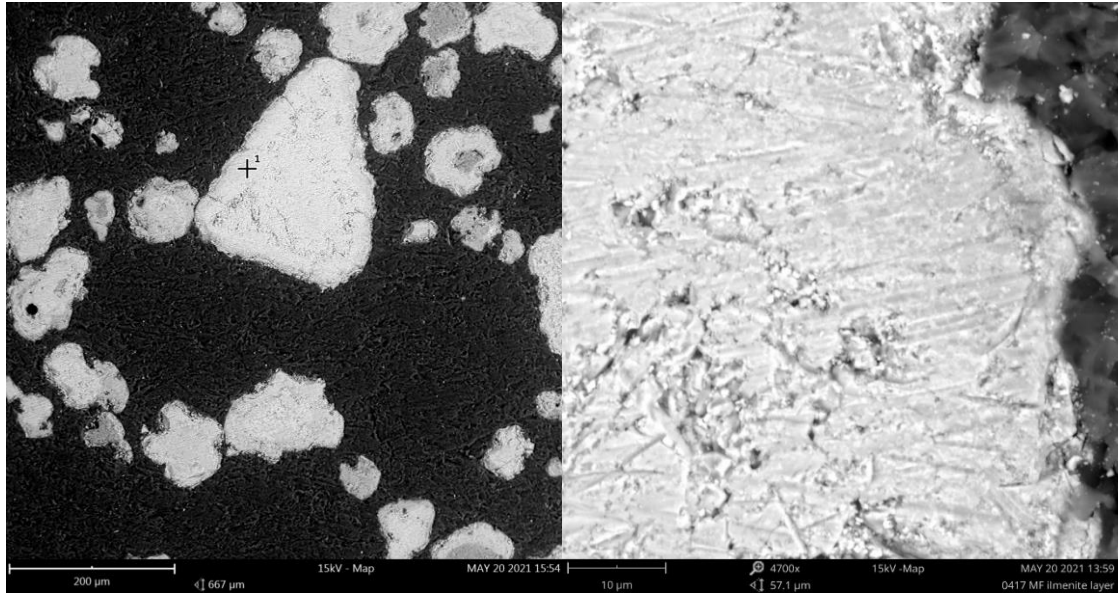
Figure 22. BS-SEM micrograph of ilmenite particle #2 (left) from the magnetic fraction (Ört-0417-MF) and surface analysed (right) in Figure 23.

Figure 22 (right) also shows an irregular surface of the ilmenite particle #2 that seems to be more heterogeneous in composition than its core.
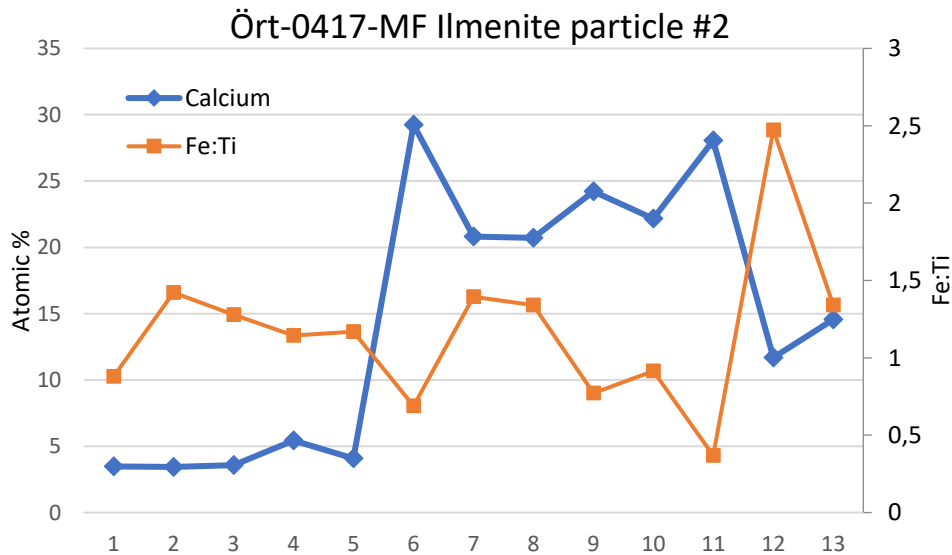
Figure 23. Fe:Ti ratio and elemental concentration of Ca in ilmenite particle #2 from Ört-0417-MF. The ratio and the concentration are plotted from a location near the core of the particle (1) to the surface of the particle (13).

As it can be observed in Figure 23, it appears again that Fe:Ti ratio shows higher values where Ca has a higher elemental concentration and vice versa. However, in this case, it can be noted that

the location where the Fe:Ti ratio rises is closer to the surface than it is for particle #1. The Fe:Ti ratio relative increase between point 1 and the point where the Fe:Ti ratio is maximum is 181.5%.

It can also be appreciated how when looking at the two closest points to the surface, particle #2 does not show an increase in Ca elemental concentration as significant as particle #1 does. This could indicate that some ash compounds that are formed on the surface are being worn off due to attrition and it will be further discussed in the Discussion section.

To observe Fe attrition, two fly ash samples from the cyclone of Chalmers boiler were analysed. As it has been said, this analysis cannot prove that attrition was happening in the Örtofta campaign, only in the Chalmers boiler. However, it is left for future work to see if both boilers showed this phenomenon and if the assumption that they can be assimilated in that sense is correct.

Since fly ash consists of smaller particles than bottom ash, following the method of taking overviews with SEM-EDS micrographs and classifying the particles with a diameter bigger than 100 μm was not a good idea. In fact, the majority of the observed particles in the fly ash that were bigger than 100 μm were ilmenite particles. What was done instead, was only trying to locate smaller particles that might give information on whether attrition was going on. In that sense, only selected particles were analysed, as the research of the composition of the fly ash was far from the objective of this project.

With this analysis some fines rich in Fe were discovered, which means that attrition of Fe was happening to some extent. The micrograph of one of these particles and its composition are represented in Figure 24 and Table 3 respectively.
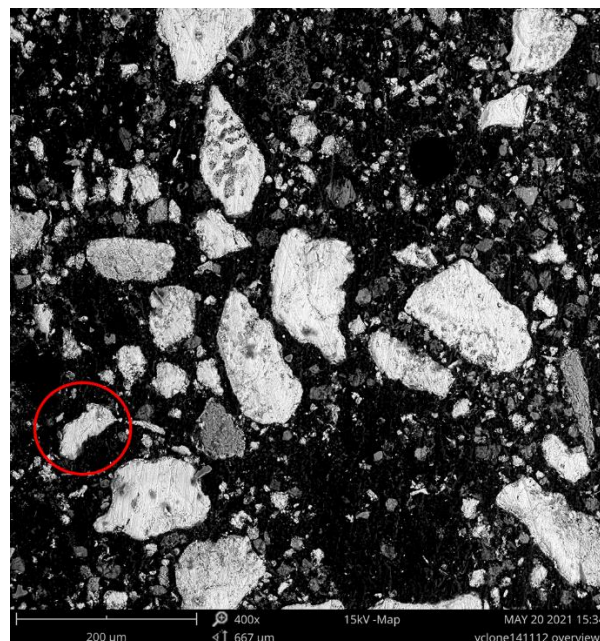
Figure 24. BS-SEM micrograph of selected Fe fine from the fly ash sample Cyk-1125-OCAC.

The highlighted particle is a fine from the oxygen carrier particles and with point analysis SEM-EDS its atomic concentration was analysed.

Table 3. Normalised elemental concentration of the highlighted particle in Figure 24 obtained with point analysis SEM-EDS.

Element	Atomic Concentration (%)
Iron	49.1
Magnesium	25.1
Titanium	11.2
Calcium	10.1
Manganese	2.1
Silicon	1.5
Potassium	1

It can be seen that the particle is indeed rich in Fe and that could mean that ilmenite particles are undergoing Fe attrition from their surfaces in the Chalmers boiler. Since only a couple of particles were selected, this analysis could be not representative for the totality of the bed and therefore attrition could be happening only for a small share of particles. It has been found that there are Fe fines in the fly ash of the Chalmers boiler and that could mean that at least a small number of particles are undergoing attrition, and the same could be happening in Kraftringen's boiler.

3.2 XRD results

In order to identify the crystalline compounds that may make these layers magnetic, XRD was performed on the same samples from Örtofta as the SEM-EDS. It can be checked which samples were analysed with each technique in the Appendix I.

XRD was used to determine which crystalline compounds are present in the samples. The result of applying the technique are the XRD scans that are shown in Figure 25.
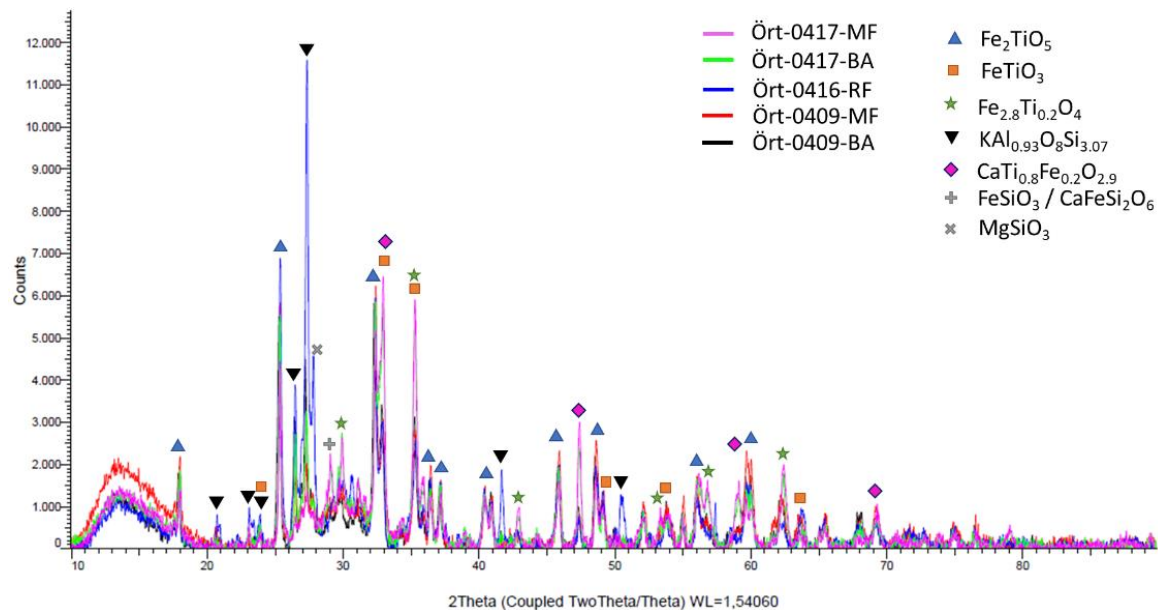
Figure 25. XRD scans for all listed samples.

The individual normalised scans (where the intensity – I in the vertical axis has been divided by the maximum intensity – I_0) can be found in Appendix IV.

The following Table 4 is a summary of the main crystalline compounds detected in each of the scans shown in Figure 25 and their relative presence, based on the relative peak intensity between the different scans.

Table 4. Crystalline compounds detected with XRD Analysis and their relative presence based on the relative peak intensity. In this table ++ indicates very high peak intensity, + indicates high peak intensity, - indicates low peak intensity and – indicates very low peak intensity.

|	Pseudobrookite (Fe$_2$TiO$_5$)	Ilmenite (FeTiO$_3$)	Magnetite / Titanomagnetite (Fe$_3$O$_4$/Fe$_{2.8}$Ti$_{0.2}$O$_4$)	K-feldspar / Microcline (KAl$_{0.93}$O$_8$Si$_{3.07}$)	Ca-titanate (CaTi$_{0.8}$Fe$_{0.2}$O$_{2.9}$)
Örtofta 0409 BA	++	+	+	-	+
Örtofta 0409 MF	++	+	+	--	+
Örtofta 0416 RF	++	+	--	+	--
Örtofta 0417 BA	++	+	++	-	++
Örtofta 0417 MF	++	+	++	--	++

Based on the identified peaks, it has been determined that pseudobrookite (Fe$_2$TiO$_5$) is present in every sample and in similar quantities. Ört-0416-RF is the sample that shows less pseudobrookite. It should be noted that the mineral phase ilmenite (FeTiO$_3$) has similar peaks as the oxidized phase and can thus overlap with pseudobrookite peaks. However, ilmenite phase is not expected to be in a significantly higher quantity than pseudobrookite after a substantial oxidation period as the one that happens in the combustor. Both phases could be present even though it could be assumed that pseudobrookite is more distributed towards the surface of the particle (as that region is oxidized faster), while ilmenite phase is distributed towards the core of the particle. Pseudobrookite also presents a slightly higher correlation to the data of the used database (Crystallography Open Database – REV212673) than ilmenite. Thus, an assumption can be made that the identified phase is primarily pseudobrookite.

There is a strong indicator that magnetite is present both in the blend before separation and in the magnetic fraction of the samples. In other words, Ört-0416-RF shows a low number of counts where the rest of the samples show magnetite peaks. Hematite shares the main peaks with magnetite and that is why, as it happens with ilmenite and pseudobrookite, it is hard to relatively quantify how much hematite there is in the samples. Magnetite still shows a considerably higher degree of correlation to the used database than hematite and that is why it is regarded as the main magnetic component of the samples.

To be able to observe the effect of operation time and magnetic separation, the normalised scans have been paired by time point of the sample in Figure 26 and by type of sample (BA, MF, RF) in Figure 27.
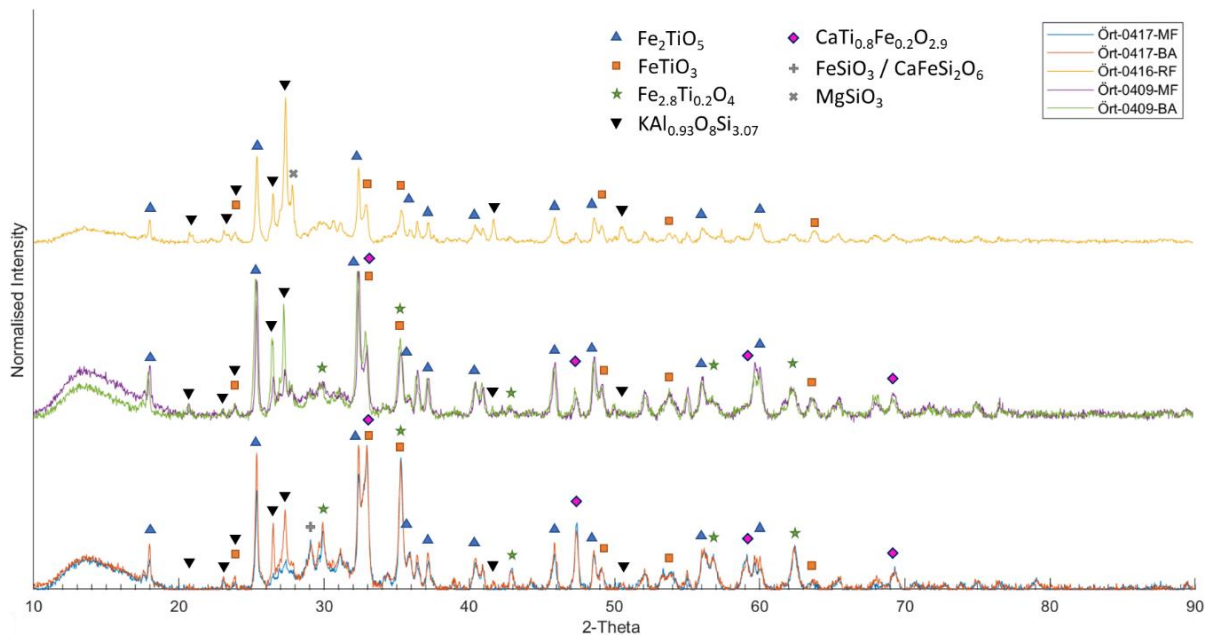
Figure 26. Normalised XRD (I/I_0) scans paired by time point.

It can be seen how there is not a significant difference between the blend and the magnetic fraction (for both days considered April 9 and 17) when it comes to the peaks that indicate the presence of magnetite. Additionally, some Fe pyroxenes ($FeSiO_3$ / $CaFeSi_2O_6$) seem to be present in the samples from April 17 and Mg pyroxene ($MgSiO_3$) could be present in the magnetic reject (Ört-0416-RF). These pyroxenes come most probably from the ashes.
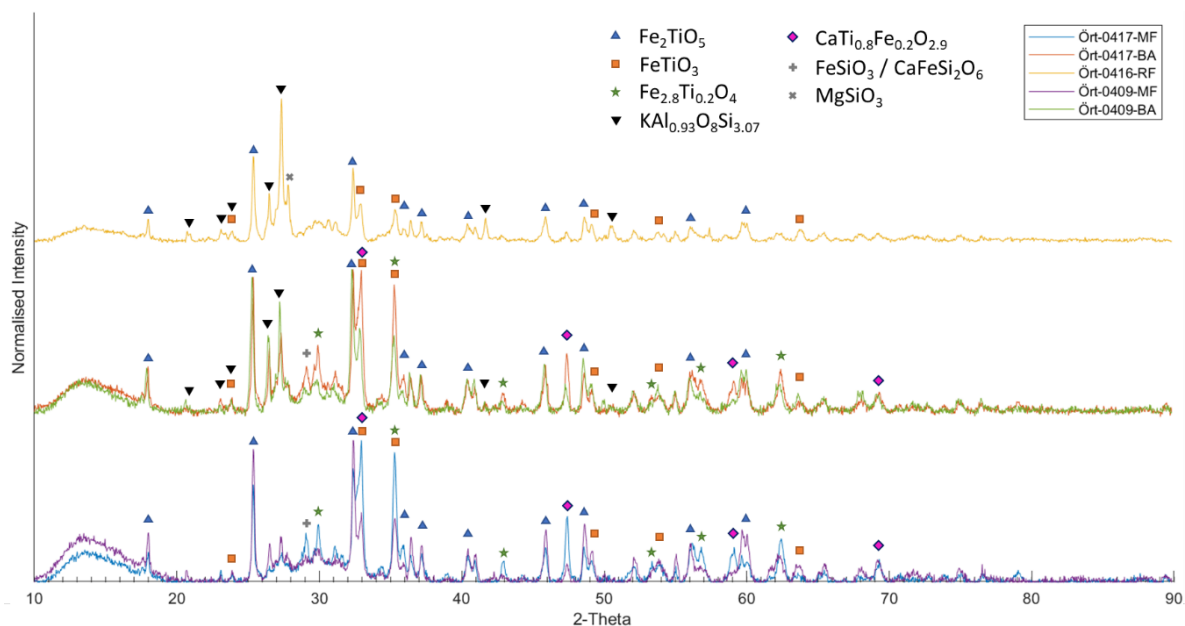
Figure 27. Normalised XRD (I/I_0) scans paired by type of sample (BA, MF, RF).

However, in Figure 27 it can be observed how both Ört-0417-MF and Ört-0417-BA have stronger peaks that relate to magnetite than their early campaign counterparts. That could suggest that, at least for this campaign, a longer residence time increases the oxidation of Fe from ilmenite towards magnetite and hematite.

Another observation when it comes to the residence time is that a Ca-titanate ($CaTi_{0.8}Fe_{0.2}O_{2.9}$) also increases its concentration with time in both the magnetic fraction and the blend. In that sense,

41

the samples from April 17 show a higher signal of this Ca-titanate than the samples from April 9. A similar compound was already present in earlier bibliography (see Corcoran et al. [16]) and the analysis shows that it can be found with high possibility both in the magnetic fraction and the blend of early of late operation days.

Regarding the magnetic reject (Ört-0416-RF), it shows a lower amount of pseudobrookite compared to the rest of the samples but there are three strong peaks that can be seen at 27.5°, 41.6° and 50.6° that are not as strong on the other samples. Those peaks indicate the presence of microcline (K feldspar). The same peaks can be seen with the blends and the magnetic fraction but the height of the peaks is considerably lower and it can be observed that the magnetic fraction has a decrease in the K-feldspar peak intensity. This last decrease is the most notable difference between the blend and the magnetic fraction (considering each pair with the same date of sampling).

3.3 Magnetic susceptibility measurements results

After the SEM-EDS and the XRD analysis, the magnetic susceptibility measurements were done for all of the samples from Örtofta from April 9, 16 and 17 that appear in Table 6 as well as for Fresh Ilmenite.

As suggested by researchers previously using the current method for magnetic susceptibility measurement, the obtained susceptibility was divided by the poured density of the sample as well as by its mass. That is because sometimes the mass specific magnetic susceptibility might not be comparable to other measured volumes or the data of other researchers [42].

The results are summarized in the following table:

Table 5. Magnetic susceptibilities measured for 5 samples obtained from Örtofta and a Fresh ilmenite sample.

Sample	Mass specific magnetic Susceptibility (m^3/kg)	Weight specific magnetic susceptibility (g^{-1})	Mass of the sample (g)
Örtofta-0417-MF	$1.38 \cdot 10^{-4}$	$1.15 \cdot 10^{-2}$	25.32
Örtofta-0417-BA	$1.20 \cdot 10^{-4}$	$1.00 \cdot 10^{-2}$	24.26
Örtofta-0409-MF	$7.68 \cdot 10^{-5}$	$6.40 \cdot 10^{-3}$	22.52
Örtofta-0409-BA	$5.91 \cdot 10^{-5}$	$4.92 \cdot 10^{-3}$	23.39
Örtofta-0416-RF	$1.82 \cdot 10^{-5}$	$1.51 \cdot 10^{-3}$	20.88
Fresh ilmenite	$3.36 \cdot 10^{-6}$	$2.80 \cdot 10^{-4}$	29.03

As it can be seen, the samples are ordered in Table 5 based on a decreasing magnetic susceptibility.

From the table, the magnetic fraction of one operation day (April 9 or April 17) can be compared with the blend of the same day and they have a magnetic susceptibility that is quite close between them (13.24% and 23.12% of relative difference respectively). It can be observed that the difference between any other pair of samples susceptibilities is higher.

This observation was somewhat expected because the magnetic susceptibility is an additive property and the compounds that are more magnetic can have a susceptibility which is several orders of magnitude higher than that of other compounds that are less magnetic (as described previously in the Magnetic separation section of the Introduction). Thus, if the magnetic

compounds account for a bigger susceptibility and they are both in the blend and in the fraction, a similar susceptibility will be measured.

Fresh ilmenite is the less magnetically susceptible sample (even less than the magnetic reject). That proves that in order to achieve magnetic separation, it is required to activate the ilmenite with several oxidizing/reducing cycles.

3.4 XRF results

XRF was the technique of choice to re-evaluate what had been observed with SEM-EDS and to try to link the chemical composition with the crystalline compound information that XRD provides and the magnetic susceptibility measurements from the Bartington sensor.

XRF has an advantage, it allows for multiple samples to be analysed simultaneously which enables the obtention of results of different samples in a short period of time. That is why the samples chosen to undergo this technique were the same 5 Örtofta samples as for the other four techniques (BS SEM, SEM-EDS, XRD, magnetic susceptibility measurements) but with the addition of two other Örtofta samples from a different time point (Ört-0413-BA and Ört-0413-MF). The information from these samples is shown in Table 6 in the Appendix I.

The samples analysed with XRF were: Ört-0409-BA, Ört-0409-MF, Ört-0413-BA, Ört-0413-MF Ört-0416-RF, Ört-0417-BA and Ört-0417-MF.

In order to have an idea of how much of the Fe was on the surface of the particles, it was decided to grind every sample and analyse twice each sample, one that had been ground and another one that had not been ground. The notation to distinguish between them is "GR" for the ground samples and no addition for the non-ground ones.

The reason for grinding is that the signal depth of XRF is limited to 1-100 μm into the particles so if the surface of the particles is made out of a Ca layer, XRF analysis will have a stronger signal coming from this element rather than from the elements located closer to the core of the particle (i.e. Ti and Fe). When grinding the samples, these layers fall off and the core is made accessible for measurement with XRF.

In the magnetic reject (Ört-0416-RF) the amount of Al, Si and K was particularly followed to see if it had any correlation to the high amounts of feldspar observed in the magnetic reject with BS SEM and SEM-EDS. Tracking the amount of Fe in every sample was also important to be able to understand what is happening with that element when ilmenite particles stay more time inside the Örtofta boiler.

As XRF takes into account the composition of the bulk phase, and not several particles like in SEM-EDS, the observations from SEM-EDS could gain strength or lose it (of course, also taking into account XRD results).

The data obtained from the XRF were spectrograms with which the XRF software can quantify the elemental composition measured in Atomic concentration. Those concentrations needed to be normalised without O and C. In the sample Ört-0413-MF GR an abnormal amount of Ce was detected and the element was excluded during the processing of the data.

After the normalisation and the adjustments were done, a list of elements ranging from 22 to 25 elements was obtained. Out of those elements, only the elements that either had a concentration higher than 1% or were present in the SEM-EDS/XRD analysis were taken into account. The elements that meet the conditions are the same elements that were found in the SEM-EDS analysis

that was done of the overviews from 5 Örtofta samples. That is: Al, Ca, Fe, K, Mg, Mn, Na, P, S, Si, Ti and Zn.

Seeking to see whether the grinding has any effect on the composition shown by XRF, each pair of ground and non-ground sample is represented in the same graph.
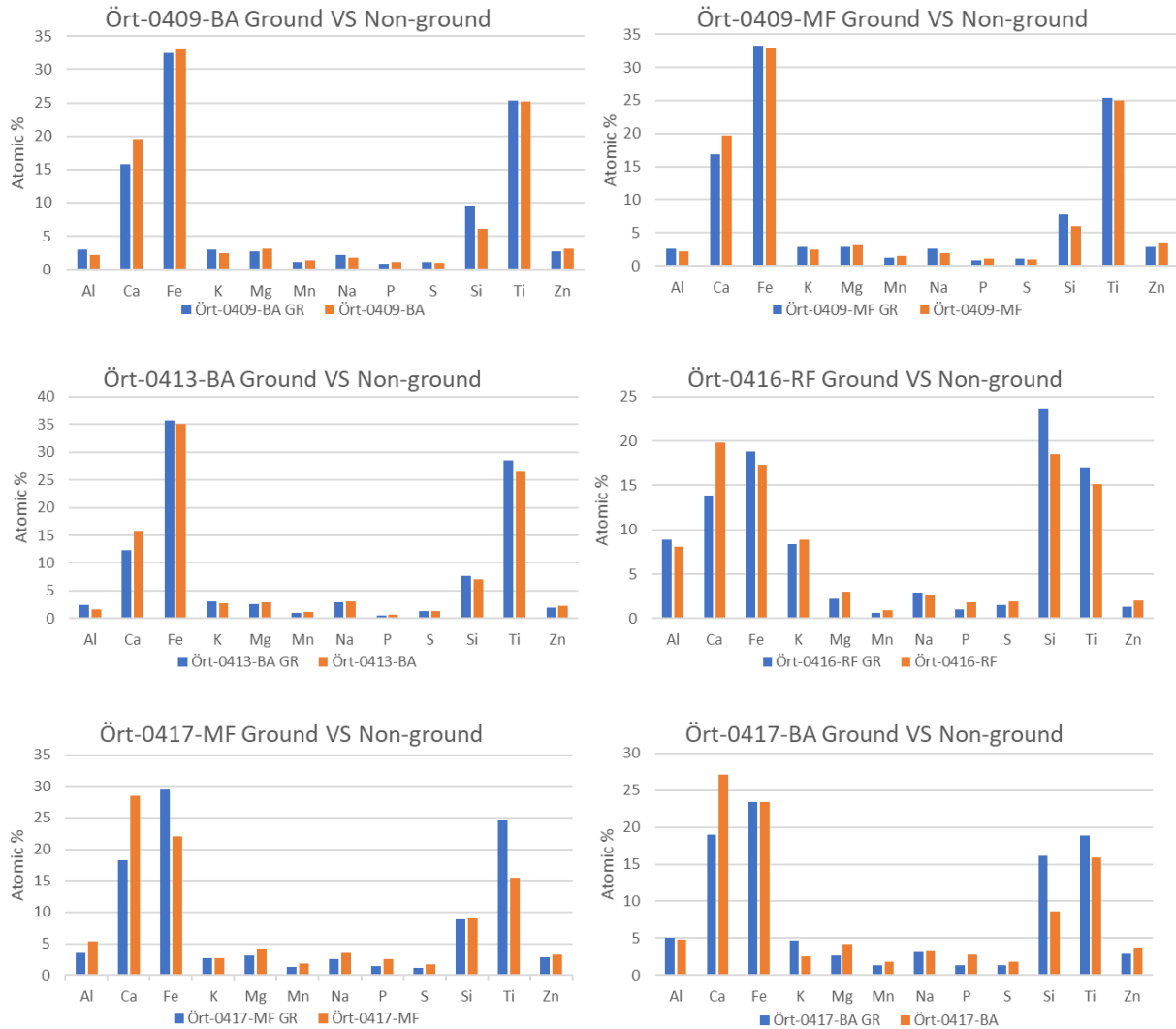
Figure 28. XRF elemental distribution comparison between the ground against the non-ground samples.

The Figure that shows the XRF elemental distribution comparison between the ground and non-ground Ört-0413-MF sample can be found in Figure 34 of the Appendix V.

The first thing that can be observed from the Figure 28 plots is the fact that the difference between the Ca concentration from a ground sample and a non-ground sample increases with time. When looking at the samples from April 9 and April 13, they differ a maximum of 3.71 percentage units, whereas when looking at the magnetic reject from April 16 (Ört-0416-RF), the blend from April 17 (Ört-0417-BA) and the magnetic fraction from April 17 (Ört-0417-MF) the difference increases up to 5.98%, 8.09% and 10.23% respectively.

44

This could mean that Ca is worn off in the process of grinding and while a higher amount of Fe and Ti is detected (which is the case), the concentration of Ca decreases. If that is the case, it would indicate that there was no migration of Ca inwards or at least it was not very significant.

The exact opposite to what happens with Ca can be argued for Ti. It can be seen how when grinding a higher % of Ti is detected. However, this difference is initially low (0.16 and 0.48 for the Ört-0409-BA and Ört-0409-MF samples respectively) and increases over time (3.03 and 9.23 for Ört-0417-BA and Ört-0417-MF respectively). This could mean that Ti, that according to the bibliography does not migrate towards the outer parts of the particle, does not migrate and a higher quantity of it is revealed when the Ca layer is worn off.

Finally, it is relevant to look at how the Fe % changes with or without grinding. For the samples from April 9 and April 13, it can be seen that it does not make a big difference as the percentage difference between the ground and the non-ground samples is low (up to 0.7% in the case of the April 13 blend - Ört-0413-BA). A considerable increase in this difference in concentration comes in the Ört-0417-MF, where Fe increases in the bulk composition by a total of 7.4% when grinding. This also could be evidence that there is a Ca layer covering the Fe and Ti from the ilmenite particles.

As it can be seen, the blends from April 9, 13 and 17 do not show a high difference between the ground samples and the non-ground ones. The same can be stated about the magnetic fractions from April 9 and April 13. That could mean that there is no Ca layer or a slim one in those samples. That is coherent considering that the April 9 and April 13 samples are from an early operation day in the campaign so the activation of the ilmenite and its migration might still be starting. It is also coherent with the fact that the blend samples present an average of the elements from all the species present in the bottom ash and thus any possible difference that could be observed is smoothed out by its diverse composition. That could be a possible explanation for the low difference in Fe % in Ört-0417-BA in comparison to the high difference shown for Ört-0417-MF.

Regarding the reject (Ört-0416-RF), even if it is from a later time point, it is not expected to have as many ilmenite particles with Fe layers in its structure in comparison to other ash compounds. The difference in Fe % in this sample is considerably lower than for Ört-0417-MF but it is higher than for Ört-0413-MF. This could mean that there is an ash layer in the reject particles but it is not as thick as the magnetic fraction one.

The comparison between ground and non-ground samples has given information on the Ca layer, but there is more information that can be extracted from the elemental composition comparison between different samples.
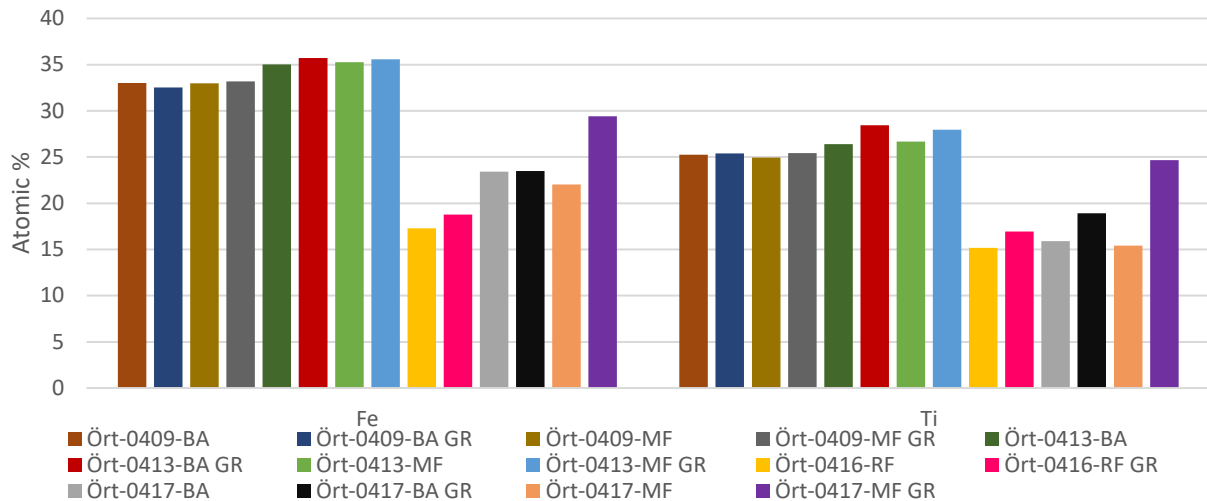
Figure 29. Atomic % distribution of Fe and Ti obtained from XRF for all listed samples.
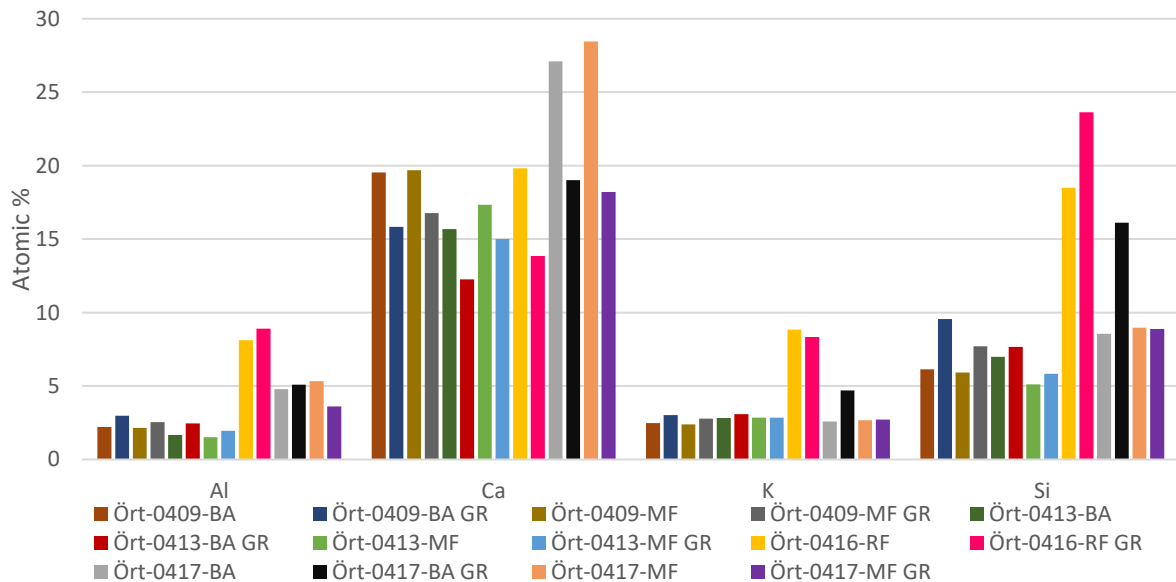
Figure 30. Atomic % distribution of Al, Ca, K and Si obtained from XRF for all listed samples.

The distribution of concentration for other minor ash elements (Na, Mg, Mn, P, S and Zn) can be found in Figures 35 and 36 in the Appendix V.

One of the first things that stands out from Figure 29 and Figure 30 is how different is the magnetic reject Ört-0416-RF from the rest of the blend and magnetic fraction samples.

The magnetic reject shows clearly a strong bulk composition in both Al, K and Si. This fact is most probably pointing directly towards the K-feldspar particles that were found in the SEM-EDS overview analysis. This confirms that there is indeed a considerable amount of feldspar in the bulk phase separated with the magnetic separation. This could clear the doubt regarding if what was observed in the SEM-EDS analysis was representative enough due to only taking into account a certain number of particles in the overviews. This sample also has the lowest % of Fe and Ti, which is in line with the fact that it should contain fewer ilmenite particles.

46

Considering Fe and Ti, it can be seen how both elements follow a similar trend in relation to the time point of each sample. There are no significant differences between the blend and the magnetic fractions for April 9 and April 13 samples, but it can be seen a slight increase in both Fe and Ti % in the April 13 samples compared to the ones extracted on April 9. A bigger change can be seen when comparing the April 13 blend and magnetic fraction with those of the April 17 time point. Both Fe and Ti decrease highly in atomic % after 4 days of operation. This decrease is more accentuated when the bottom ash blend from April 17 is considered, which is coherent with the fact that it has a diverse composition and that ash compounds increase with time of operation. This overall decrease in Fe and Ti in 4 days of operation could mean that ash is accumulating and that this could be reduced by increasing the ilmenite feeding rate.

When the blend Ört-0417-BA is ground it can be seen how the bulk concentration of Al, Si and K increases. All the other minor elements that come from the ash of the fuel and are represented in Figures 35 and 36 in the Appendix V do not show this increase in composition when being ground. A similar observation can be made with the magnetic reject Ört-0416-RF, except for K, whose concentration diminishes when being ground.

Another important observation that could be important for other alkali uptake studies is the fact that for the blend and magnetic fraction samples, the amount of K is quite evenly distributed between the different time points and the ground and non-ground samples. The only exception to that is the April 17 ground BA blend (Ört-0417-BA GR). Of course, the K signal could be driven by the feldspar of the samples but either way, this could be interesting for alkali uptake studies.

4 Discussion

In this section of the report a general overview of the results will take place and some hypotheses that were stated at the start of the Results section will be confirmed, denied or commented on. Furthermore, a connection between the results as well as possible inconsistencies will be traced.

First of all, with SEM-EDS it was observed that the longer the operation time is, the higher is the concentration increase in elements coming from the ash (Ca, K, Si and so forth) in the ilmenite particles. This means that as it was known from past bibliography and presented in the introduction, ilmenite reacts with the ashes of the fuel resulting in an uptake of these elements in the form of new compounds.

One of the compounds that has been identified thanks to the XRD analysis is the Ca-titanate $CaTi_{0.8}Fe_{0.2}O_{2.9}$. This compound had previously been found in earlier research by Corcoran et al. [21], which is present in the bibliography of this report. In that research paper, it was stated that $CaTi_{0.7}Fe_{0.3}O_{2.5}$ (which is similar in composition) was found in a rock ilmenite OCAC campaign in the Chalmers CFB boiler. This titanate was referred to as $CaTiO_3$ in a more recent publication from Corcoran et al. [16]. The suggested mechanism of formation for the compound in the paper stated that it accumulated on the surface and Ca^{2+} migrated inwards reacting with TiO_2 and therefore being incorporated into the ilmenite structure. It was seen how this Ca-titanate was capable of forming inner layers that were differentiated from the outer ones. The main difference was the heterogeneity of composition in the outer layer, that presented many other ash elements, while the inner layer was more homogeneous.

The results of the present report can confirm that there is a Ca layer in some of the ilmenite particles of the latest time point analysed (April 17). First, the BS SEM micrographs of two selected ilmenite particles from the magnetic fraction Ört-0417-MF (Figures 20 and 22) show that from a morphological standpoint, the surfaces of the particles appear to be irregular and more heterogeneous. This heterogeneity in composition is confirmed by SEM-EDS, that shows an increase in concentration of Ca in the surface of the particle when successive point analysis are used for characterizing it (Figures 21 and 23).

With SEM-EDS, the two ilmenite particles of Ört-0417-MF were analysed and both of them appeared to show the presence of a Ca layer. However, there were differences between the layers of these two particles. For particle #1, it appeared to be a double layer on both sides of a Fe rich region that could be an Fe layer, something that was also observed in the bibliography and that will be further discussed afterwards. For particle #2, there was a high Fe concentration in points immediately close to the surface and a Ca rich region appeared below that Fe rich region.

The possible explanation for this discrepancy could be the attrition of the outer ash layer. The SEM-EDS data suggests that there is an accumulation of Ca on the surface of ilmenite particles and then Ca^{2+} migrates inwards forming the Ca-titanate that was detected with XRD analysis, resulting in an inner layer that is incorporated in the ilmenite structure. The outer ash layer could be removed from the particle due to attrition forces, leaving the possible Fe layer in the surface of particle #2 and the inner Ca layer immediately below. According to this, ilmenite particle #1 would have not undergone attrition of the outer Ca layer or at least the attrition of the layer would be only partial.

Given that in the Örtofta boiler there was a periodic renewal of bed material with ilmenite, it could be that particle #1 had less residence time in the boiler than particle #2 and thus it was less sensible to attrition forces.

This could be corroborated with an analysis of the fly ash of the Örtofta campaign, but since it was not available, it will be left for future work. However, attrition in OC beds which have been operating for many hours is a common event. It is the case for Ört-0417-MF, which was taken around 300 hours of operation, according to the industrial partner.

It has not been proven for the Örtofta campaign, but it has been proven earlier in this report that there was Fe attrition in the fly ash from the Chalmers boiler samples that were extracted from the cyclone during a 2014 winter campaign. In order to see attrition of Fe, there has to be also a removal of the outer ash layer of the particles (if the particle presents such layer). Fe attrition was also observed by Corcoran et al. [16] in less operation time (72 hours). Therefore, attrition of the ash layer can be expected as an explanation for the removal of the Ca layer of particle #2.

The presence of a Ca layer has also been proven with XRF as the ground Ört-0417-MF sample shows a significant decrease in bulk Ca concentration and an increase in Ti and Fe concentration. This means that while Ca was worn off from several particles, Fe and Ti were revealed on the surface and XRF could detect a higher quantity of those elements (due to analysis depth limitations of the instrument).

However, with XRF it has not been proven that there is an inner layer, as the decrease in the concentration of Ca is not coherent with that statement. Ca migration inwards cannot be proven with that technique although the technique does not deny that it could be happening. The possible explanations are that the particles that have been ground have been removed from every possible layer (i.e. Fe layer, outer and inner Ca layer) or that the migration has happened very slowly and thus only a thin and low concentration Ca layer is formed, which does not make a difference when accounting for the total bulk concentration of the element.

The finding of both the Ca layer and the identification of the compound as a Ca titanate that is similar to the one present in the bibliography, as well as the suggestion that the mechanism for the layer build-up could be similar is very interesting. That is because Kraftringen's boiler is an industrial boiler which is considerably bigger than the Chalmers semi-industrial scaled boiler, and the fuel with which it was fired in that campaign (wood pellets and waste wood) was more heterogeneous than the fuel which is used in the Chalmers boiler (wood pellets). When burning waste wood, it is expected to work with a more diverse composition of the ash than when burning wood pellets, whose main ash components are Ca and K. Since both fuels are woody biomass, it is expected to observe a high uptake of Ca and K in the ilmenite particles.

Following the observations regarding this Ca layer, it seems that the other ash elements present in the Örtofta fuel (Na, Al, S, P and so forth) do not modify significantly the Ca outer layer build-up mechanism from the previous observations made by other researchers (such as [16]).

According to the SEM-EDS analysis of the surface of an ilmenite particle from the reject, there is also an outer Ca layer on the reject OC particles. XRF analysis also seems to indicate that there is some type of outer Ca layer attached to the surface of the particle. However, XRD did not identify the Ca-titanate ($CaTi_{0.8}Fe_{0.2}O_{2.9}$) in the reject, so it has to be in the form of another compound. The fact that no inner layer was observed on the reject particles and no Ca-titanate was detected supports that the Ca-titanate has to intervene in the suggested mechanism of migration of Ca^{2+} inside the particles from the magnetic fraction Ört-0417-MF, where inner layers were observed with SEM-EDS.

The Ca-titanate compound is not the only compound that comes with the fuel ashes that has been identified in this report. K-feldspar ($KAl_{0.93}O_8Si_{3.07}$), Mg pyroxenes ($MgSiO_3$) and Fe pyroxenes ($FeSiO_3$ / $CaFeSi_2O_6$) have also been identified.

The K-feldspar particles were the first artifacts detected in the experimental part. The presence of feldspar in the particles was detected with SEM-EDX and it was confirmed with the XRD and XRF analysis that there is feldspar in all samples, but especially in the magnetic reject Ort-0416-RF. This feldspar mainly comes from the fuel, as the fresh ilmenite only shows traces of feldspar attached to the ilmenite particles that are there because of the way the ore is mined. Furthermore, the share of these gangue minerals in the fresh ilmenite is very low according to the classification that can be seen in Table 2 of the SEM-EDS results (approximately 2%).

As it was expected, the magnetic species present in the blend of the bottom ashes dictate the magnetic properties of it and that is proved by the fact that between BA and MF there is no big difference in the value of the magnetic susceptibility. With this, it can be stated that effectively feldspar does not have a major impact on the magnetic susceptibility of the samples and thus the magnetic separator is extracting the majority of it. A hypothesis that has not been proved and will be left for future work is if the feldspar particles present in the magnetic fraction are in some way covered by a magnetic compound.

In the magnetic fraction (Ört-0417-MF), SEM-EDS particle analysis detected that the surface of a feldspar particle had an increase in the concentration of Fe, Ti and Ca. With BS SEM a clear layer of different composition could be observed in Figure 16. With XRF it has been seen that when the particles from the reject (Ört-0416-RF) are ground, the concentration of Al, K and Si increases, which could be suggesting that there is also a layer on the feldspar particles from the sample (as feldspar is composed of those three elements). It would be interesting to investigate in future work if K-feldspar can develop a layer from Fe or ash fines and whether the Fe compound present in it shows magnetic properties or has an oxygen carrier ability.

The reduction in Fe concentration in the XRF analysis of Ört-0417-MF and Ört-0417-BA in comparison with the blend and the magnetic fraction obtained in both April 9 and April 13 could indicate three things. Firstly, it could mean that the decrease in Fe and Ti is due to the fact that more and more ash compounds are getting accumulated in the samples and therefore the bulk concentration of those elements decreases. Secondly, it could mean that there is indeed Fe migration towards the surface of the particle and attrition (therefore, a loss of Fe). This explanation would not explain why there is also a decrease in Ti concentration. Thirdly, it could be that both previous explanations are true and both ash accumulation and Fe attrition are happening.

The SEM-EDS analysis of two ilmenite particles from the magnetic fraction (Ört-0417-MF), which can be seen in Figures 21 and 23, shows that there is an Fe rich region close to the surface that could be a result of Fe migration. This Fe migration would result in the formation of oxygen-carrying Fe oxides during the oxidation of free Fe. Titanomagnetite has been found with XRD and hematite is also there (even if hard to quantify) so a case can be made for Fe migrating outwards and being oxidized to oxygen-carrying Fe oxides which are more magnetic than ilmenite, according to Table 1.

Regarding the magnetization of the samples, it has been proven that with residence time the ilmenite particles become more magnetically susceptible and thus, more sensitive to a magnetic separation with a magnetic pulley. The value of the magnetic susceptibility for the latest magnetic fraction available (Ört-0417-MF) is $1.38 \cdot 10^{-4}$ m^3/kg which almost fits between the magnetic susceptibility interval for titanomagnetite ($1.69 \cdot 10^{-4} - 2.9 \cdot 10^{-4}$ m^3/kg) given by the bibliography chosen as reference (Table 1). The value is also close in magnitude to those of magnetite ($3.9 \cdot 10^{-4} - 5.8 \cdot 10^{-4}$ m^3/kg), which appears in the same Table 1. This means that there is magnetite in the sample as it is the only expected magnetic Fe oxide that can show such ferrimagnetic levels of magnetic susceptibility because hematite and ilmenite have much lower susceptibilities.

Thanks to the detection of the titanomagnetite compound in XRD, it can be suggested that the main source of that increase in magnetism is the oxidation that the free Fe in the samples undergoes in order to become magnetite. It could be argued that there is hematite in the sample because the most important peaks of that compound are close to the magnetite peaks in the XRD scans, but magnetite has a higher correlation with the database, it fits a higher number of peaks and according to the values of magnetic susceptibility obtained, it is a proven fact that it has to be in the sample. Both oxides are probably present in the particle the same way that there is probably a mixture of pseudobrookite and ilmenite phase in the sample, as the particles are never totally oxidized or reduced.

The fact that for the same time point the blend and the magnetic fraction do not have a magnetic susceptibility that differs as much as with every other combination of two samples means that whatever the amount of ash compounds there are in the sample, the magnetic compounds with better magnetic properties of the sample (magnetite in this case) dictate its susceptibility, which is something that was expected. Thus, it can be concluded that the ash layers in the particles do not interfere highly in the magnetic separation efficiency as the separation is mainly dictated by the main magnetic compounds (i.e. titanomagnetite). That is why an ash layer has been observed both in the ilmenite particles from the reject (Ört-0416-RF) and the magnetic fraction (Ört-0417-MF).

The presence of magnetite also supports the fact that the main ilmenite phase obtained in the XRD analysis was pseudobrookite instead of ilmenite as it is the oxidized phase and by April 17 several oxidizing cycles had already passed. Of course, it is hard to quantify the presence of one with respect to the other so there are most likely both at the same time. The presence of pseudobrookite also means that probably there is also hematite in the samples and it is not detected in the susceptibility measurements because magnetite's susceptibility "masks" hematite's contribution to the bulk susceptibility.

One thing that stands out from the magnetic susceptibility measurements of the fresh ilmenite is how low is its magnetic susceptibility. The value is $3.36 \cdot 10^{-6}$ m^3/kg and it is slightly higher than the one that appears in the bibliography ($1.7 \cdot 10^{-6}$, $2 \cdot 10^{-6}$). This low value means that there is no mineral titanomagnetite present in the fresh ilmenite. That verifies that titanomagnetite is formed through oxidation, following the reaction R11 shown in the "Fe magnetic phases" section of the Introduction. In Karlsson [32] it was observed how the magnetic separation (%) was correlated to the magnetic susceptibility of ilmenite particles that had been used in a 12 MW^{th} boiler (OCAC) while being fed wood chips or pellets (same boiler and same fuel as in the studied cyclone samples). In that study two possible reasons for ilmenite particles increased magnetic behaviour were given:

1. Fresh ilmenite was received in a reduced state and used ilmenite had gone through oxidation, forming hematite and magnetite which are more magnetic than fresh ilmenite.
2. Fe migrates to the surface of the particles while undergoing redox cycles. While doing so, Fe concentration increases and pure Fe oxides with high magnetic susceptibility are formed.

One of them or both could also be true for the present case. The migration of Fe, even though not proved by XRF, could still be happening as discussed earlier. The oxidation of ilmenite towards magnetic oxides is happening as the XRD peaks showing titanomagnetite/hematite paired by type of sample (BA, MF or RF) in Figure 27 show higher peaks when referring to late time points (i.e. higher overall residence time). One of the two phenomena or both were occurring in the Örtofta boiler from April 4 to April 22 of 2018.

Even though Fe migration has not been proved by all techniques, a suggested explanation for the increase in magnetic susceptibility in this report is that Fe migrates towards the surface of the rock ilmenite particle, where the oxygen partial pressure is higher, and then is oxidized into hematite and magnetite, which show higher magnetic susceptibilities than fresh ilmenite.

Regarding the magnetic separation efficiency, it should be taken into account that if not enough fresh material is fed or not enough bottom ash is magnetically separated, ilmenite particles will start to add more and more ash compounds to its structure. The problem is that those particles, no matter how much ash they have incorporated in the form of Ca-titanates, Fe pyroxenes or other compounds, will become more and more magnetically susceptible. At least that can be stated when considering the span of time from April 9 to April 17 from that exact Örtofta campaign. The particles will become more susceptible even if overall Fe concentration is decreasing (it is not possible to say that Fe is being lost here due to attrition as it has not been proven). Supposing Fe also migrates towards the surface in the ilmenite particles from Örtofta and the particles are undergoing attrition, as long as new free Fe keeps being oxidized to magnetite those particles will still be magnetically separated.

This can be positive if the positive effects of larger residence times and ash uptake are considered, like reduction of the corrosion due to K uptake. However, it can also be negative if the negative impact is highlighted, like the increase in Fe attrition due to particle porosity increasing. This means that there is a time window regarding the extraction in which the magnetic separation has a positive impact and increases the efficiency of the process when considering ash uptake and oxygen carrying capacity.

The separation should be performed once ilmenite has been activated and is susceptible enough to be separated. The activation time is dependent on the fuel and the operational conditions of the boiler. It should also be thoroughly combined with regeneration of the material so that it is made sure that the magnetic separation is not only separating ilmenite particles with lower and lower oxygen carrying ability (once attrition starts to happen) with thick ash layers attached to them. The separation should not be delayed until those effects start to have a negative impact on the overall efficiency of the oxygen carrier bed material inside the combustor.

If the amount of fresh ilmenite added is excessive or the magnetic separation is handled before the fresh material particles have been activated, a considerable amount of fresh ilmenite particles could go into the reject due to not showing the magnetic susceptibility needed in order to be separated. If that is the case, fresh material could be lost before being used. This exact thing would explain why there were some big ilmenite particles with few ash elements in their composition in the shares of the magnetic reject. These ilmenite particles were the artifacts that were presented in the reject and were noticed with the share classification of particles with SEM-EDS. Those particles resembled fresh ilmenite in their composition and that is because most probably they were ilmenite particles that had been recently added before the point of extraction. Those particles had not been activated and therefore they did not have oxygen carrying oxides such as magnetite or hematite in their structure. These particles probably had a slightly higher magnetic susceptibility than fresh ilmenite and that is why they could not make it to the magnetic fraction.

That way, magnetic separation has to be timed correctly in order to not lose unexploited material and to make sure that the one that is being used allows for the best performance possible. There is a preferred time window regarding the extraction that could be theoretically optimized by incorporating magnetic susceptibility measurements in the plant in order to have more insight on when it is adequate to apply the magnetic separation and consequent recirculation of bed material or when it is better to feed more fresh ilmenite. The magnetic susceptibility method used in this

report is non-invasive and is based on manual extraction of samples but it could be automated which could make it fitting for application in industry.

Furthermore, in this report, it has been observed that along with activation of the particles, a higher magnetization is accomplished. That happens, presumably, until Fe attrition of the particles provokes the decrease of oxygen carrying capacity. If that is the case, an interesting follow-up for this report would be the investigation of the connection between oxygen carrying capacity and magnetic susceptibility measurements. The investigation on bulk magnetic susceptibility as a predictor or an indicator of oxygen carrying capacity could be very helpful towards accomplishing higher efficiency of magnetic separation in OCAC.

5 Future work

The first thing that can be proposed as future work is the repetition of the measurements and characterizations done in this report. As it was said when introducing the experimental part, the boiler located at Örtofta has a high capacity (60 tonnes) and in comparison, the number of particles analysed with XRF and magnetic susceptibility was small. A yet smaller number of particles were analysed with XRF and SEM-EDS, and therefore, the conclusions drawn for this small number of particles could not represent the entire sample or what had happened in the boiler. It was assumed that the combination of the methods used in this report could adequately represent the whole, but it needs to be verified with further experimentation. Especially the conclusions that were drawn based of particle analysis with SEM-EDS will need to be revisited to check that they were representative.

Other analysis techniques or even other modes of operation of the techniques used in this report could be used in order to obtain more information about the samples. SEM-EDS, for example, could be used in the mode that obtains intensity maps to gain information about whole particles and not only parts of them. That could allow for easier characterization of the particles and a better understanding of how the different element concentrations are distributed through the bed material particles.

Another possible improvement that could be done in future work is the addition of more magnetic reject samples, as the present report only treated one. The sample was indeed different to the other samples, so the magnetic separation had effectively been applied and it can be appreciated but the comparison with other magnetic rejects would give more information about the efficiency of the separation and the conditions of the particles that end up in the reject.

The samples analysed only with XRF (Ört-0413-BA and Ört-0413-MF) could be analysed with XRF, BS SEM, SEM-EDS and their magnetic susceptibilities could be measured. This was not done due to time constraints but it could be done to complement the information of the April 9 and April 17 time points with another time point that is equally distant to both. If obtained, the fly ash samples from the Örtofta facility could also be analysed to check the Fe attrition and when does it appear.

As commented already in the Discussion, the feldspar particles present in the magnetic accept show a Fe-Ti-Ca layer whose properties (magnetic susceptibility and oxygen carrying capacity) would be interesting to see.

The alkali uptake of the particles from Örtofta could be investigated as XRF showed a quite stable bulk concentration of the particles across the samples except for the magnetic reject. K intensity

maps could be taken of the particles to see the K distribution in the particle, as the presence of feldspar in the bulk phase of the samples complicates drawing conclusions with XRF.

An interesting continuation of the report would be measuring the oxygen carrying capacity of the samples with TGA (Thermogravimetric Analysis) or in a small boiler in order to correlate it to what has been observed through the report. As it has been said in the Discussion, another potentially interesting route to follow after this project would be looking into the correlation between bulk magnetic susceptibility and the oxygen carrying capacity of the particles. The potential use of magnetic susceptibility as a predictor or indicator of the oxygen carrying capacity could be very promising if proven. A model could be adjusted between the two variables and the correlation coefficient (R^2) could be obtained. If one would like to take it a step further, that model could be trained with data from the regular extractions of the plant applying Machine Learning, so that the resulting model could help in decision making regarding the proper time of extraction of material, magnetic separation and recirculation.

Last but not least, the investigation conducted in this report could be done with other particles from other industrial plants or other campaigns from the same CHP plant so that the observations could be compared or maybe general trends could be observed.

6 Conclusions

In this Bachelor thesis, the magnetically separated samples from an OCAC campaign in Kraftringen's CHP plant located in Örtofta have been investigated. The blend before separation, the magnetic fraction and the magnetic reject have been subjected to a morphological and chemical characterization with BS SEM and SEM-EDS. The crystalline compounds present in each sample have been identified with XRD and their bulk composition has been characterized with XRF. In order to correlate the chemical composition of the samples with the residence time in the boiler and their magnetic susceptibility, magnetic susceptibility measurements have been also carried out.

A classification of particles analysed in each sample with SEM-EDS gave the share of ilmenite particles, feldspar particles, particles that derived from ilmenite or had a high ash elements concentration and other particles. Feldspar particles that come from the fuel were observed as artifacts in the magnetic fraction, covered in an Fe-Ti-Ca layer, according to SEM-EDS analysis.

Operation time allowed the formation of Ca layers in the ilmenite particles of the magnetic fraction. SEM-EDS analysis of two particles from the sample showed the formation of a double layer around a possible Fe layer in one of the particles and a single inner layer below another possible Fe layer on the other particle. The most probable explanation for the difference between the two layers was attrition forces that wore off the outer ash layer of the particle with only an inner one. The mechanism of migration for the Ca^{2+} to form such inner layers could be assimilated to the one present in previous bibliography, as according to XRD analysis the compound formed is $CaTi_{0.8}Fe_{0.2}O_{2.9}$, similar to other Ca-titanates reported in the bibliography. The proposed mechanism consists in Ca deposition in the surface and diffusion inwards to react with TiO_2 and be incorporated in the ilmenite structure as the identified Ca-titanate.

Also, with an increase in operation time (i.e. in average residence time of the bed material) an increase in mass specific magnetic susceptibility was observed for the magnetic blend and the magnetic fraction. That is mainly due to the formation of magnetic Fe oxides such as titanomagnetite (ferrimagnetic) and hematite (antiferromagnetic), identified with XRD. A mechanism for the formation of these oxides was suggested. The mechanism finds its support in the SEM-EDS finding of possible Fe layers in the surface of ilmenite particles from the magnetic fraction of the sample with the latest time point. This mechanism should be re-evaluated with other techniques.

The proposed mechanism of formation of the oxides starts with Fe^{2+} migration towards the surface of the particle, where the oxygen partial pressure is higher, and where it is oxidized to form magnetite and if further oxidized it forms hematite.

The magnetic susceptibility of the ilmenite particles seems to increase with residence time and an initial stage of activation is required in order to present the Fe oxides that show the susceptibility needed for magnetic separation. A preferred time window for the separation was presented. An early separation and recirculation will result in ilmenite particles showing low magnetic susceptibilities, similar to the ones measured for fresh ilmenite ($3.36 \cdot 10^{-6}$ m^3/kg), which leads to the particles ending in the magnetic reject. A late separation and recirculation will result in ilmenite particles becoming increasingly magnetic, even though the oxygen carrying capacity is being diminished due to Fe attrition and thick ash layers are being formed around the particle.

Therefore, the process of separation and recycling has to be timed correctly in order to not lose fresh material or recirculate material with low oxygen carrying capacity. Magnetic susceptibility

measurements are suggested as a useful tool in decision making regarding the adequate time of the separation and its consequent recirculation.

References

[1]   NASA's Global Climate Change, "Overview: Weather, Global Warming and Climate Change." https://climate.nasa.gov/resources/global-warming-vs-climate-change/ (accessed May 11, 2021).

[2]   WWF Australia, "Impacts of global warming.", [Online]. Available: https://www.wwf.org.au/what-we-do/climate/impacts-of-global-warming#gs.12eft9 (accessed May 11, 2021).

[3]   U.S. Energy Information Administration, "Energy and the environment explained - Where greenhouse gases come from," 2020, [Online]. Available: https://www.eia.gov/energyexplained/energy-and-the-environment/where-greenhouse-gases-come-from.php (accessed May 21, 2021).

[4]   P. Friedlingstein *et al.*, "Global Carbon Budget 2020," *Earth System Science Data*, vol. 12, no. 4, pp. 3269–3340, 2020, doi: 10.5194/essd-12-3269-2020.

[5]   C. Le Quéré *et al.*, "Fossil CO2 emissions in the post-COVID-19 era," *Nature Climate Change*, vol. 11, no. March, 2021, doi: 10.1038/s41558-021-01001-0.

[6]   P. Agreement and U. Nations, "Paris agreement," 2015, [Online]. Available: https://unfccc.int/files/essential_background/convention/application/pdf/english_paris_agreement.pdf.

[7]   R. Rohde, "Berkeley Earth January 2021 Temperature Update," *Berkeley Earth,* [Online]. Available:. http://berkeleyearth.org/january-2021-temperature-update/#:~:text=Global Summary&text= (accessed Apr. 21, 2021).

[8]   T. Mauritsen and R. Pincus, "Committed warming inferred from observations," vol. 7, no. July, pp. 1–5, 2017, doi: 10.1038/NCLIMATE3357.

[9]   S. V Vassilev, D. Baxter, and C. G. Vassileva, "An overview of the behaviour of biomass during combustion: Part I. Phase-mineral transformations of organic and inorganic matter," *Fuel*, vol. 112, pp. 391–449, 2013, doi: 10.1016/j.fuel.2013.05.043.

[10]   S. V Vassilev, C. G. Vassileva, Y. Song, W. Li, and J. Feng, "Ash contents and ash-forming elements of biomass and their significance for solid biofuel combustion,", *Fuel*, vol. 208, pp. 377–409, 2017, doi: 10.1016/j.fuel.2017.07.036.

[11]   A. Gyllén, *Oxygen carrier aided combustion : Implementation of oxygen carriers to existing industrial settings*. 2019.

[12]   A. Lyngfelt, A. Brink, Ø. Langørgen, T. Mattisson, M. Rydén, and C. Linderholm, "11,000 h of chemical-looping combustion operation — Where are we and where do we want to go?," *International Journal of Greenhouse Gas Control*, vol. 88, no. May, pp. 38–56, 2019, doi: 10.1016/j.ijggc.2019.05.023.

[13]   F. Störner, F. Hildor, H. Leion, M. Zevenhoven, L. Hupa, and M. Rydén, "Potassium Ash Interactions with Oxygen Carriers Steel Converter Slag and Iron Mill Scale in Chemical-Looping Combustion of Biomass-Experimental Evaluation Using Model Compounds," *Energy and Fuels*, vol. 34, no. 2, pp. 2304–2314, 2020, doi: 10.1021/acs.energyfuels.9b03616.

[14]   F. Hildor, M. Zevenhoven, A. Brink, L. Hupa, and H. Leion, "Understanding the interaction of potassium salts with an ilmenite oxygen carrier under dry and wet conditions," *ACS Omega*, vol. 5, no. 36, pp. 22966–22977, 2020, doi: 10.1021/acsomega.0c02538.

[15]   D. Filippou and G. Hudon, "Iron removal and recovery in the titanium dioxide feedstock and pigment industries," *JOM*, vol. 61, no. 10. pp. 36–42, 2009, doi: 10.1007/s11837-009-0150-3.

[16]   A. Corcoran, P. Knutsson, F. Lind, and H. Thunman, "Mechanism for Migration and Layer Growth of Biomass Ash on Ilmenite Used for Oxygen Carrier Aided Combustion," *Energy and Fuels*, vol. 32, no. 8, pp. 8845–8856, 2018, doi: 10.1021/acs.energyfuels.8b01888.

[17]   C. Guizani, M. Jeguirim, S. Valin, L. Limousy, and S. Salvador, "Biomass chars: The effects of pyrolysis conditions on their morphology, structure, chemical properties and reactivity," *Energies*, vol. 10, no. 6, 2017, doi: 10.3390/en10060796.

[18]   P. Knutsson and C. Linderholm, "Characterization of ilmenite used as oxygen carrier in a 100 kW chemical-looping combustor for solid fuels," *Applied Energy*, vol. 157, pp. 368–373, 2015, doi: 10.1016/j.apenergy.2015.05.122.

[19]   D. Bhogeswara Rao and M. Rigaud, "Kinetics of the oxidation of ilmenite," *Oxidation of Metals*, vol. 9, no. 1, pp. 99–116, 1975, doi: 10.1007/BF00613496.

[20]   X. Fu, Y. Wang, and F. Wei, "Phase transitions and reaction mechanism of ilmenite oxidation," *Metallurgical and Materials Transactions A: Physical Metallurgy and Materials Science*, vol. 41, no. 5, pp. 1338–1348, 2010, doi: 10.1007/s11661-010-0173-y.

[21]   A. Corcoran, J. Marinkovic, F. Lind, H. Thunman, P. Knutsson, and M. Seemann, "Ash properties of ilmenite used as bed material for combustion of biomass in a circulating fluidized bed boiler," *Energy and Fuels*, vol. 28, no. 12, pp. 7672–7679, 2014, doi: 10.1021/ef501810u.

[22]   I. Staničić, "Fate of Trace Elements in Thermochemical Conversion of Waste Fuels Using Oxygen Carriers," p. 24, 2021, [Online]. Available: https://research.chalmers.se/en/publication/523712%0Ahttps://research.chalmers.se/publication/523712/file/523712_Fulltext.pdf.

[23]   W. J. Bronkala, "Magnetic separation," in *Ullmann's Encyclopedia of Industrial Chemistry*, Wisconsin: Wiley, 2000, pp. 133–144.

[24]   PowderProcess.net, "Industrial Magnet traps and separators for powder - A guide to magnetic separation.", [Online]. Available: https://www.powderprocess.net/Equipments html/Magnets.html (accessed May 15, 2021).

[25]   J. Svoboda, "Magnetic Separation," in *Encyclopedia of Materials: Science and Technology*, Elsevier, 2005, pp. 1–7.

[26]   J. A. Oberteuffer, "Magnetic Separation: A Review of Principles, Devices, and Applications," *IEEE Transactions on Magnetics*, vol. 10, no. 2, pp. 223–238, 1974, doi: 10.1109/TMAG.1974.1058315.

[27]   C. Kittel and S. Johnson, *Introduction to Solid State Physics*, 8th Edition Berkeley: John Wiley & Sons Inc, 2004.

[28]   W. D. Callister and D. G. Rethwisch, *Materials Science and Engineering: An Introduction*, 8th Edition Wiley, 2010.

[29]   J. Dearing, *Environmental Magnetic Susceptibility - Using the Bartington MS2 system*, 2nd Edition Bartington, 1999.

[30]   A. Gupta and D. Yan, *Mineral Processing Design and Operations*, 2nd Edition Elsevier, 2016.

[31] J. D. Steenkamp and P. C. Pistorius, "Reflections on ilmenite roasting and magnetic separation," in *Heavy minerals conference proceedings*, 2005, no. July 2017, pp. 133–141.

[32] F. Karlsson, "Magnetic separation of oxygen carriers from bed ash in heat and power plants," 2019.

[33] M. Ezzahmouly *et al.*, "Micro-computed tomographic and SEM study of porous bioceramics using an adaptive method based on the mathematical morphological operations," *Heliyon*, vol. 5, no. 12, p. 3, 2019, doi: 10.1016/j.heliyon.2019.e02557.

[34] J. I. Goldstein *et al.*, *Scanning Electron Microscopy and X-ray Microanalysis*, 3rd Edition New York: Springer, 2003.

[35] S. E. Dann, *Reactions and Characterization of Solids*. Cambridge: Royal Society of Chemistry, 2000.

[36] A. H. Simon, *Sputter Processing*. Elsevier Inc., 2018.

[37] ThermoFisher Scientific - Ask A Scientist Staff, "What is XRF (X-ray Fluorescence) and How Does it Work?," 2020, [Online]. Available: https://www.thermofisher.com/blog/ask-a-scientist/what-is-xrf-x-ray-fluorescence-and-how-does-it-work/ (accessed May 13, 2021).

[38] A. Barhoum, M. L. García-Betancourt, H. Rahier, and G. Van Assche, *Physicochemical characterization of nanomaterials: Polymorph, composition, wettability, and thermal stability*. Elsevier Inc., 2018.

[39] Yale University West Campus Materials Characterization Core, "XRF - Principle," 2021, [Online]. Available: https://ywcmatsci.yale.edu/gallery/xrf/principle (accessed May 13, 2021).

[40] C. J. Dixon, "The Tellnes Ilmenite Deposit - Norway," in *Atlas of Economic Mineral Deposits*, Dordrecht: Springer, 1979, pp. 108–109.

[41] L. G. Woodruff, G. M. Bedinger, and N. M. Piatak, "Titanium Chapter T of Critical Mineral Resources of the United States — Economic and Environmental Geology and Prospects for Future Supply Professional Paper 1802 – T U.S. Department of the Interior," *U.S. Deparment of the Interior - U.S. Geological Survey*, no. Professional Paper 1802–T, p. 26, 2017, doi: https://doi.org/10.3133/ pp1802T.

[42] "Personal communication with researchers from Improbed AB.", 2021.

Appendix I. Code used for the samples

The following Table 6 (in the next page) shows all the samples that were analysed with each technique along with where they were obtained from and the time in which they were extracted from the boiler. A code has been designed for a conciseness matter. The code consists of the following terms:

$$ABC - MMDD - Type$$

Where *ABC* is based on the first three letters of the name of the place where the sample was extracted, *MMDD* is the date or timestamp of obtention of the sample (month and day) and *Type* consists of additional information, e.g. the indication on whether the sample is the blend that has not undergone magnetic separation (BA), the magnetic fraction (MF) or the magnetic reject fraction (RF) of the bottom ash (BA) sample. On the date of obtention the year is omitted because the samples of interest are from the same origin (Örtofta) and since all of them share the same year of operation, adding the year does not give any new information.

The notation for the additional information stands for the following:

- BA: Bottom Ash collected directly from the boiler and that has not undergone magnetic separation. It is the blend that would go into the magnetic separator.
- MF: Magnetic fraction obtained from the introduction of the bottom ash blend (BA) in the boiler.
- RF: Reject fraction obtained from the introduction of the bottom ash blend (BA) in the boiler.
- OCAC: It just identifies that the sample has been used for OCAC in the Chalmers boiler.

Table 6. List of all the samples analysed with SEM-EDS techniques.

Code	Name of the sample	Place of origin	Timestamp of obtention of the sample	SEM-EDS	XRD	χ measurements	XRF
Fresh ilmenite	Fresh ilmenite	Titania mine, Norway (Chalmers)	Season 2016 (spring)	X		X	
Ört-0409-BA	Örtofta 180409	Örtofta Improbed	2018-04-09	X	X	X	X
Ört-0409-MF	Örtofta 180409 magnetic fraction	Örtofta Improbed	2018-04-09	X	X	X	X
Ört-0416-RF	Örtofta 180416 magnetic reject	Örtofta Improbed	2018-04-16	X	X	X	X
Ört-0417-BA	Örtofta 180417	Örtofta Improbed	2018-04-17	X	X	X	X
Ört-0417-MF	Örtofta 180417 magnetic fraction	Örtofta Improbed	2018-04-17	X	X	X	X
Ört-0413-BA	Örtofta 180413	Örtofta Improbed	2018-04-13				X
Ört-0413-MF	Örtofta 180413	Örtofta Improbed	2018-04-13				X
Cyk-1117-OCAC	Sekcyklon 141117 OCAC 7.09	Chalmers Boiler	2014-11-17	X			
Cyk-1125-OCAC	Sekcyklon 141125 OCAC 6.40	Chalmers Boiler	2014-11-25	X			

Appendix II. Specific methodologies followed for SEM-EDS

When taking the 6 overviews from the Örtofta samples and the fresh ilmenite a specific order was followed to avoid bias in the selection of the locations. The next Figure 31 illustrates how that was handled.
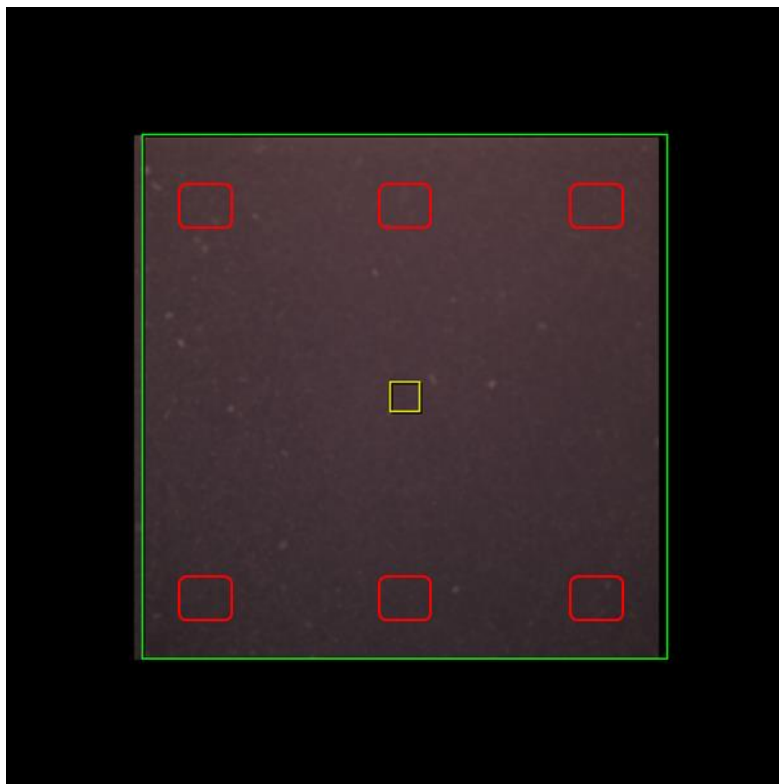
Figure 31. Illustration of where the overviews were taken for particle share quantification. Sample shown: Ört-0409-BA.

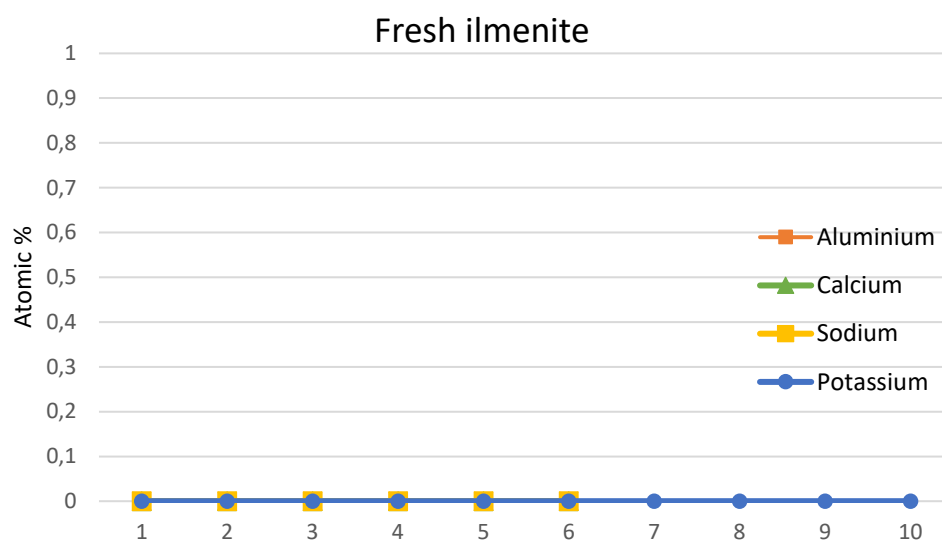# Appendix III. Additional Figures for the layer analysis with SEM-EDS

Figure 32. Elemental distribution for Fresh ilmenite particle. The distribution of Al, Ca, Na and K is plotted from the surface of the particle to a location near its core.

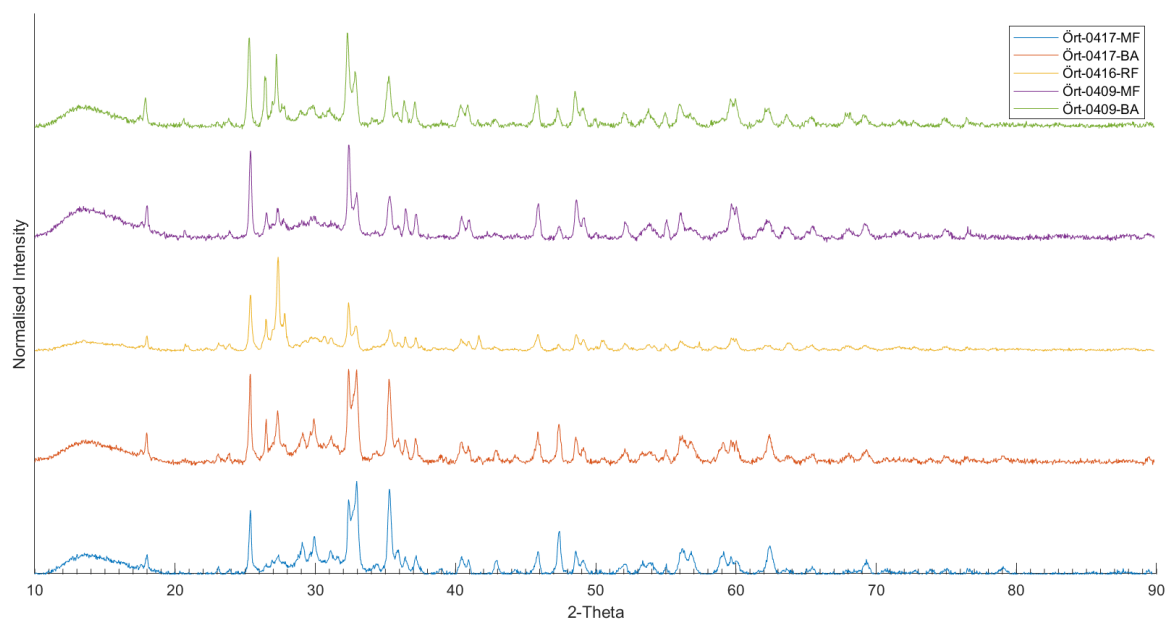# Appendix IV. Additional Figures for the XRD scans

Figure 33. Normalised XRD (I/I₀) scans.
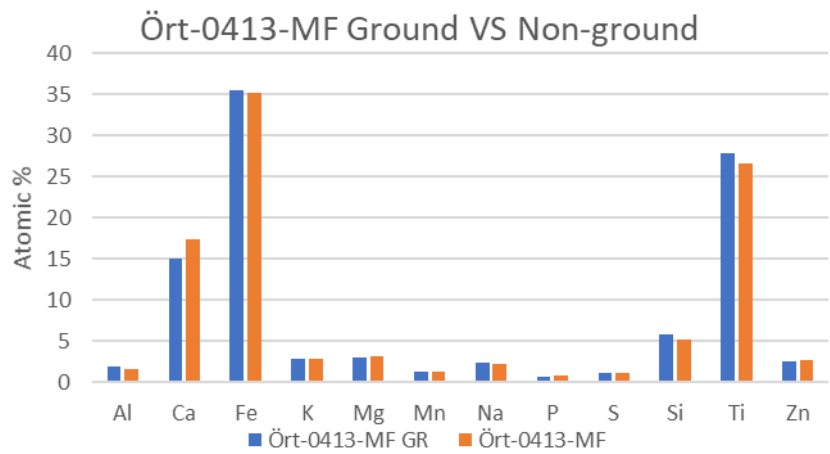
Appendix V. Additional Figures for the XRF results

Figure 34. XRF elemental distribution comparison between the ground against the non-ground Ört-0413-MF sample.
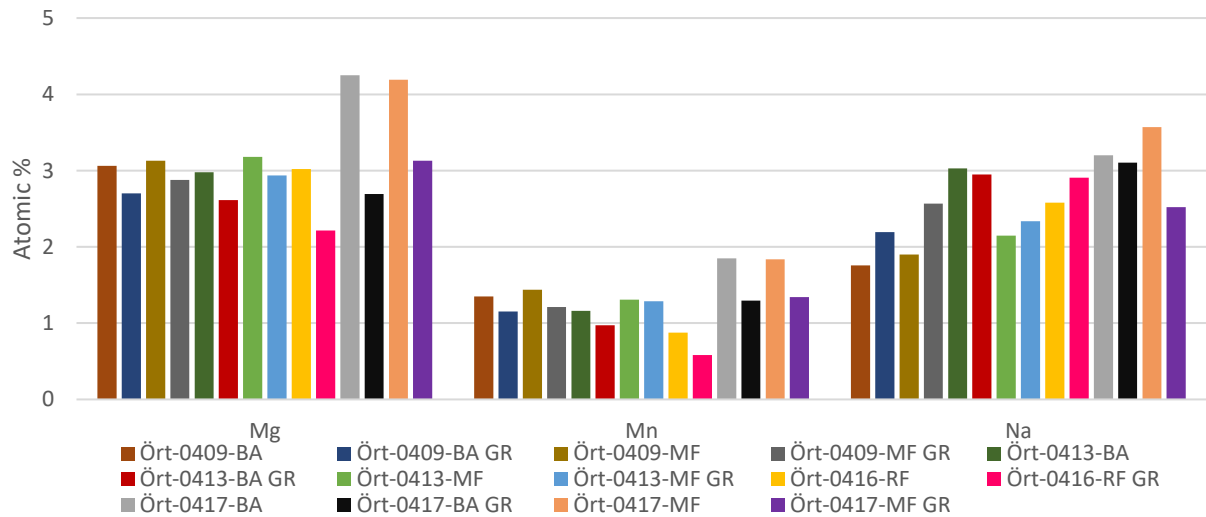

Figure 35 Atomic % distribution of Mg, Mn and Na obtained from XRF for all listed samples.
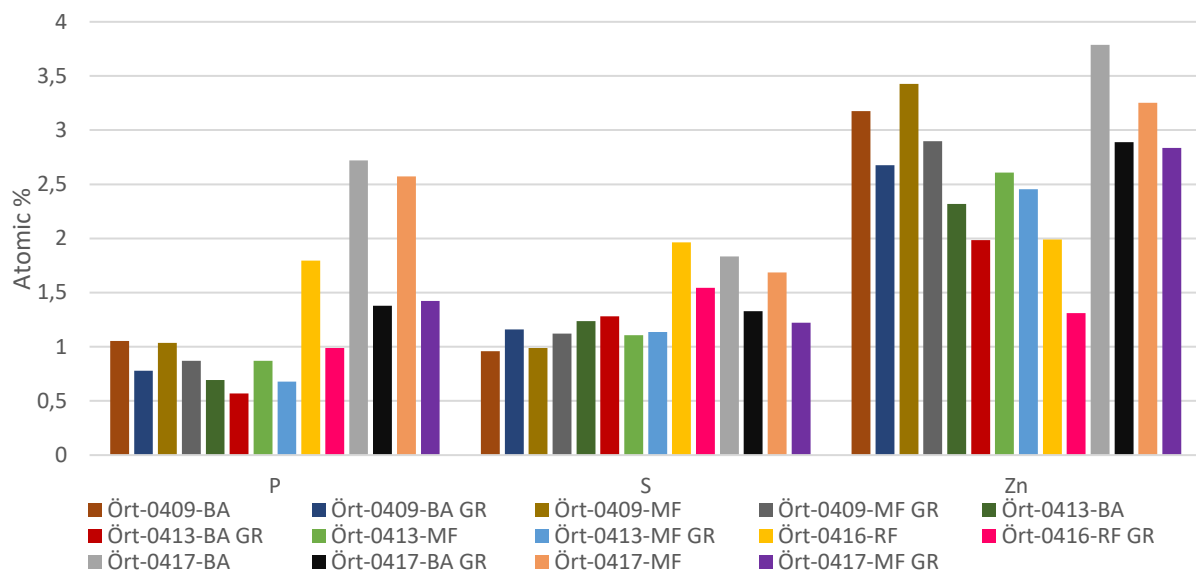
Figure 36. Atomic % distribution of P, S and Zn obtained from XRF for all listed samples.